PNNL-13369

Pacific Northwest
National Laboratory
Operated by Battelle for the
U.S. Department of Energy

Waste Form Release Calculations for the 2001 Immobilized Low-Activity Waste Performance Assessment

D. H. Bacon
B. P. McGrail

February 2001

Prepared for the U.S. Department of Energy
under Contract DE-AC06-76RL01830

DISCLAIMER

PACIFIC NORTHWEST NATIONAL LABORATORY
operated by
BATTELLE
for the
UNITED STATES DEPARTMENT OF ENERGY
under Contract DE-AC06-76RL01830

Printed in the United States of America

Available to DOE and DOE contractors from the
Office of Scientific and Technical Information,
P.O. Box 62, Oak Ridge, TN 37831-0062;
ph: (865) 576-8401
fax: (865) 576-5728
email: reports@adonis.osti.gov

Available to the public from the National Technical Information Service,
U.S. Department of Commerce, 5285 Port Royal Rd., Springfield, VA 22161
ph: (800) 553-6847
fax: (703) 605-6900
email: orders@ntis.fedworld.gov
online ordering: http://www.ntis.gov/ordering.htm

This document was printed on recycled paper.
(2/01)

PNNL-13369

Waste Form Release Calculations for the 2001 Immobilized Low-Activity Waste Performance Assessment

D. H. Bacon
B. P. McGrail

February 2001

Prepared for
the U.S. Department of Energy
under Contract DE-AC06-76RL01830

Pacific Northwest National Laboratory
Richland, Washington 99352

Summary

A set of reactive chemical transport calculations was conducted with the Subsurface Transport Over Reactive Multiphases (STORM) code to evaluate the long-term performance of a representative low-activity waste glass in a shallow subsurface disposal system located on the Hanford Site. One-dimensional simulations were conducted out to times in excess of 20,000 yr. A two-dimensional simulation was run to 2,000 yr. The maximum normalized Tc release rate from a trench-type conceptual design under a constant recharge rate of 4.2 mm/yr is 0.93 ppm/yr. Factors that were found to significantly impact the predicted release rate were water recharge rate, chemical affinity control of glass dissolution rate, diffusion coefficient, and disposal system design (trench versus a concrete-lined vault). In contrast, corrosion of the steel pour canister surrounding the glass waste and incorporation of a chemical conditioning layer of silica sand at the top of the trench had little impact on Tc release rate. However, because of large inventory of Cr associated with the 304L steel containers and assumed short release time (1000 yr) relative to the glass, a four orders of magnitude higher release rate of Cr(VI) was predicted relative to the ILAW glass alone.

Contents

Figures

Tables

Introduction

The Hanford Site in southeastern Washington State has been used extensively to produce nuclear materials for the U.S. strategic defense arsenal by the U.S. Department of Energy (DOE). A large inventory of radioactive and mixed waste has accumulated in 177 buried single- and double-shell tanks. Liquid waste recovered from the tanks will be pretreated to separate the low-activity fraction from the high-level and transuranic wastes. The low-activity waste (LAW) will be immobilized in glass and placed in a near-surface disposal system on the Hanford Site. Vitrifying the LAW will generate over 160,000 m^3 of glass. The immobilized low-activity waste (ILAW) at Hanford is among the largest volumes of waste within the DOE complex and is one of the largest inventories of long-lived radionuclides planned for disposal in a low-level waste facility (approximately 2.4 million curies total activity). Before the ILAW can be disposed, DOE must approve a performance assessment (PA), which is a document that describes the long-term impacts of the disposal facility on public health and environmental resources. A sound scientific basis for determining the long-term release rates of radionuclides from LAW glasses must be developed if the PA is to be accepted by regulatory agencies, stakeholders, Native Americans, and the public.

Approach and Rationale

The 1998 version of the ILAW PA (Mann et al. 1998) showed that one of the key variables in the analysis is the waste form release rate, which must be calculated over thousands of years. To conduct this calculation, we used a methodology where the waste form release rate is evaluated by modeling the basic physical and chemical processes that are known to control dissolution behavior instead of using empirical extrapolations from laboratory "leaching" experiments commonly used in other performance assessments. We adopted this methodology for the following reasons:

- The dissolution rate, and hence radionuclide release rate from silicate glasses is not a static variable, i.e., a constant that can be derived independent of other variables in the system. Glass dissolution rate is a function of three variables (neglecting glass composition itself): temperature, pH, and composition of the fluid contacting the glass (McGrail et al. 2001). The temperature of the ILAW disposal system is a known constant. However, both pH and composition of the fluid contacting the glass are variables that are affected by flow rate, reactions with other engineered materials, gas-water equilibria, secondary phase precipitation, alkali ion exchange, and by dissolution of the glass itself (a classic feedback mechanism). Consequently, glass dissolution rates will vary both in time and as a function of position in the disposal system. There is no physical constant such as a "leach rate" or radionuclide release rate parameter that can be assigned to a glass waste form in such a dynamic system.

- One of the principal purposes of the ILAW PA is to provide feedback to engineers regarding the impacts of design options on disposal system performance. A model based on empirical release behavior of the waste form could not provide this information. For example, we have found little effect on waste form performance regardless of whether stainless or cast steel is used for the waste form pour canister. However, significant impacts have been observed when large amounts of concrete are used in constructing vaults for ILAW. The concrete raises the pH of the pore water entering the waste packages and so increases glass corrosion.

Unfortunately, the robust methodology we used does not come without additional requirements. First, detailed information is needed regarding the reaction mechanisms controlling the dissolution behavior of the waste form. Significantly more laboratory experiments are required to obtain the rate law parameters needed for the models used for our simulations. Second, the model now being used (described in the next section) is markedly more complex because of its ability to simulate reactive transport coupled with heterogeneous, unsaturated flow. Execution times with today's fastest workstations can take weeks for one-dimensional (1-D) and two-dimensional (2-D) simulations, and three-dimensional (3-D) simulations can be attempted only on today's most sophisticated massively parallel computers. Still, we believe the benefits, particularly with regards to the technical defensibility of the methodology and results, far outweigh the penalties.

Computer Model Selection

The code selection criteria and selection process used is documented in *Selection of a Computer Code for Hanford Low-Level Waste Engineered-System Performance Assessment* (McGrail and Bacon 1998). The needed capabilities were identified from an analysis of the important physical and chemical processes expected to affect LAW glass corrosion and the mobility of radionuclides. The available computer codes with suitable capabilities were ranked in terms of the feature sets implemented in the code that match a set of physical, chemical, numerical, and functional capabilities needed to assess release rates from the engineered system. The highest ranked computer code was found to be the STORM code developed at Pacific Northwest National Laboratory (PNNL) for DOE for evaluation of arid land disposal sites. The verification studies for STORM are documented in *Subsurface Transport Over Reactive Multiphases (STORM): A General, Coupled Nonisothermal Multiphase Flow, Reactive Transport, and Porous Medium Alteration Simulator, Version 2, User's Guide* (Bacon et al. 2000).

Methods

Model Setup and Parameterization

This section details the data used in the STORM code input data file (Bacon et al. 2000). Input data to STORM can be conveniently divided into two parts: 1) unsaturated flow and transport, and 2) chemistry. Entries for unsaturated flow and transport include: 1) lithographic units, 2) hydraulic properties, 3) hydraulic initial conditions, and 3) hydraulic boundary conditions. These data were principally defined from facility design documents (Puigh 1999), the near-field hydraulic properties data package (Meyer and Serne 1999), or the far-field hydraulic properties data package (Khaleel 1999). STORM was used to compute the flow-field in the near-field region based upon hydraulic properties for the materials, and specified initial and boundary conditions. Chemistry input to STORM consists of entries for 1) aqueous species, 2) gas species, 3) solid species, 4) equilibrium reactions, 5) kinetic reactions, and 6) geochemical initial and boundary conditions. Each of these inputs is described below.

Unsaturated Flow and Transport Input

Lithographic Units

To establish a consistent framework for overlaying a computational grid on the spatial domain of interest, a set of material zones or lithographic units are established with similar hydrogeological and geochemical properties. These zones are usually related to disposal design components, geologic formations, or geologic facies determined from borehole analyses. However, because there are practical limits to the resolution of the model grid, material zones may also include combinations of materials that are assigned uniform hydraulic and/or chemical properties. Classification of these materials into appropriate zones was performed as a part of the near-field hydraulics data package (Meyer and Serne 1999).

The remote-handled (RH) trench simulations encompass a 1-D vertical profile near the center of a single trench (Figure 1). It is assumed that the material representing the waste packages is 85% glass and 15% filler by volume. For the new ILAW vault simulations, waste packages with 85% glass and 15% filler by volume (Figure 2) were also assumed. The principal differences between the cases involve the incorporation of degraded concrete layers at the top and bottom of the ILAW vault and thinner layers of filler between waste package layers.

For each lithographic unit, a list of the solid species that comprise the unit is required. For each solid, the following data is needed:

- Relative volume
- Particle radius

Figure 1. Lithographic Units for Remote-Handled (RH) Trench Waste Form Release Simulations

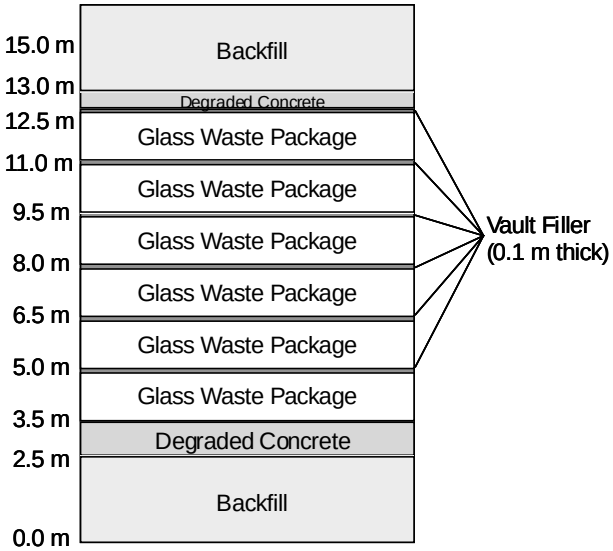

Figure 2. Lithographic Units for New ILAW Vault Waste Form Release Simulations

Values for these variables for each lithographic unit are listed in Table 1 and Table 2. The waste package is assumed to consist of 304L stainless steel container filled with LAWABP1 waste glass. For Hanford sands, backfill soil, petrologic, and particle size data was obtained from the near-field hydrology data package (Meyer and Serne 1999). For the vault simulations, the filler material between waste packages is assumed to be quartz sand. The vault concrete is assumed to consist of back-filled soil mixed with 15% Portland cement. Other materials in the simulations include vault concrete, backfill, Hanford Sand, vault filler, and additional solid phases. For the RH trench simulations, the backfill material is assumed to consist of 40% albite, 40% quartz, 10% K-feldspar, and 10% illite (Mann et al. 1998). Degraded vault concrete is assumed to consist of backfill with 15% Portlandite added. The vault filler and Hanford Sand were assumed to have the same mineral composition as the backfill material.

Table 1. Relative Volume of Solid Species in Material Zones

	ILAW Glass	**304L ss**	**Quartz**	**Albite**	**K-Feldspar**	**Illite**	**Portlandite**
Waste Package	0.99	0.01	0	0	0	0	0
Filler	0	0	1	0	0	0	0
Vault Concrete	0	0	0.34	0.34	0.085	0.085	0.15
Back-filled Soil	0	0	0.4	0.4	0.100	0.100	0
Hanford Sands	0	0	0.4	0.4	0.100	0.100	0

The assumed particle radius values for Hanford sediments and backfill soil are consistent with petrologic and particle size data obtained from laboratory-measured values (Kaplan and Serne 1999). The particle size of the filler material between waste packages is assumed to be the same as that for the backfill soil. For the Portland cement, we have simply assumed that the material is heavily degraded into

Table 2. Particle Radius (m) of Solid Species in Material Zones

	ILAW Glass	304L ss	Quartz	Albite	K-Feldspar	Illite	Portlandite
Waste Package	5.00E-02	5.00E-02		0	0	0	0
Filler	0	0	1.00E-04	0	0	0	0
Vault Concrete	0	0	1.00E-04	1.00E-04	1.00E-04	5.00E-06	1.00E-04
Back-filled Soil	0	0	1.00E-04	1.00E-04	1.00E-04	5.00E-06	0
Hanford Sands	0	0	1.00E-04	1.00E-04	1.00E-04	5.00E-06	0

rubble (Krupka and Serne 1998) with consistency similar to surrounding soil. Comparatively, the glass is assumed to have an average 500 times larger radius. This is consistent with the expected sparse degree of glass fracturing in the waste package based on prior experience with high-level waste glasses (Farnsworth et al. 1985; Peters and Slate 1981). Fracturing is expected to increase the glass surface area a maximum of 10X over its geometric surface area.

Computational Grid

The computational grid was set at 5 cm in vertical resolution; this is slightly larger than the 3.66 cm grid spacing used in the 1998 ILAW PA. The time step used in the calculations was calculated automatically by the code given a convergence criterion of $1x10^{-6}$. This ensures that predicted values of aqueous species concentrations and mineral volumes are accurate between iterations for a given time step. If this cannot be achieved within a certain number of iterations, the time step is automatically reduced. Numerous simulations were conducted to ensure that the grid spacing and convergence criteria chosen for the simulations were small enough to ensure accuracy, yet large enough to allow the simulations to finish in a reasonable amount of time. For comparison, the base case remote-handled trench simulation was rerun with a grid spacing of 2.5 cm, and with a convergence criterion of $5x10^{-7}$. Results from these simulations were not significantly different from the results reported herein.

Material Hydraulic Properties

The hydraulic properties for each lithographic unit in the simulation were defined as a part of the near-field hydraulics data package (Meyer and Serne 1999), or the far-field hydraulic properties data package (Khaleel 1999) but are provide in Table 3 for convenience.

Hydraulic Initial Conditions

Initial hydraulic conditions for each lithographic unit include the following parameters:

- Water content
- Water flux
- Dissolved gas content of aqueous phase
- Gas pressure

- Relative humidity of gas phase
- Temperature

Table 3. Material Hydraulic Properties Used In Simulations

Material	Particle Density (g/cm^3)	Bulk Density (g/cm^3)	Saturated Water Content	Residual Water Content	van Genuchten α (cm^{-1})	van Genuchten *n*	Saturated Hydraulic Conductivity (cm/s)
Vault Concrete	2.63	2.46	0.067	0.00	3.87×10-5	1.29	1.33×10^{-9}
Vault Filler	2.63	1.59	0.397	0.005	0.106	4.26	3.79×10^{-2}
Glass Waste	2.68	2.63	0.020	0.00	0.200	3.00	0.01
Backfill	2.76	1.89	0.316	0.049	0.035	1.72	1.91×10^{-3}
Conditioning Layer	2.63	1.59	0.397	0.005	0.106	4.26	3.79×10^{-2}
Degraded Concrete	2.76	1.89	0.313	0.00	2.43	1.41	1.34×10^{-3}
Hanford Sand	2.74	1.71	0.375	0.041	0.055	1.77	2.88×10^{-3}

The initial conditions were calculated by assuming a steady state water flux at the upper boundary, which results in a steady state water content distribution consistent with the hydraulic properties defined for each material. A wide spectrum of water flux rates, ranging from 0.1 mm/y to 50 mm/y were used for different sensitivity cases. A constant subsurface temperature, equal to the average ambient temperature of 15°C was assumed. The dissolved gas content of the aqueous phase was assumed to be negligible with respect to flow. The relative humidity of the gas phase was assumed to be 100%.

Hydraulic Boundary Conditions

The following data is needed as a function of time and space along each boundary:

- Water flux
- Dissolved gas content of aqueous phase
- Gas pressure
- Relative humidity of gas phase
- Temperature

The upper boundary is located just beneath the engineered barrier system (EBS) and was assigned a specified flux. A wide spectrum of water flux rates, ranging from 0.1 mm/y to 50 mm/y were used for different sensitivity cases. The ambient recharge rates, 0.9 or 4.2 mm/y, were determined as a part of the recharge data package (Fayer et al. 1999). The lowest recharge rate of 0.1 mm/y represents a perfectly working EBS. The highest recharge rate (50 mm/y) represents the highest probable flux running off the edge of the EBS.

The location of the lower boundary was selected so that vertical gradients are small. For the trench simulations, the lower boundary is a free drainage boundary 4.5 m below the lowest layer of backfill. For the vault simulations, the lower boundary is a free drainage boundary 2.5 m below the lowest layer of concrete. For hydraulic boundary conditions at this lower boundary, free drainage under gravity will be assumed. For two-dimensional simulations, the side boundaries are placed at axes of symmetry so that they can be assumed to be no-flow boundaries.

A constant subsurface temperature, equal to the average ambient temperature of 15°C was assumed. The dissolved gas content of the aqueous phase was assumed to be negligible with respect to flow. The relative humidity of the gas phase was assumed to be 100%.

Solute Transport Coefficients

For each gaseous and aqueous species, the following data is needed:

- Aqueous diffusion coefficient ($m^2\ s^{-1}$)
- Gas diffusion coefficient ($m^2\ s^{-1}$) or an assumption that the gas partial pressure is fixed

The aqueous diffusion coefficients were assumed to be $5x10^{-9}$ m^2/s for all aqueous species (Mann et al. 1998). The gas partial pressure for CO_2 and O_2 were fixed at atmospheric values of $3x10^{-4}$ and $2.1x10^{-1}$ atm, respectively.

Chemistry Input

Aqueous Species

Aqueous species are the cations, anions, or neutral complexes present in the aqueous phase. For each aqueous species, the following data is needed:

- Molecular Weight
- Charge
- Hard core diameter
- Number of elements in aqueous species
- Stoichiometric coefficient of each element

The aqueous species listed in Table 4 were identified by simulating the dissolution of LAWABP1 glass (along with a trace amount of calcite) in deionized water at 15°C with the EQ3/6 code package (Wolery and Daveler 1992). All data were obtained from the EQ3/6 data0.com.R8 database (Daveler and Wolery 1992). These simulations were not intended to be representative of disposal system conditions. The intent was only to make use of the EQ3/6 software to extract a subset of aqueous (and solid) species from the large thermodynamic database that were relevant for ILAW simulations. Since LAWABP1 glass contains all of the elements that are currently expected to be part of the final ILAW

Table 4. Key Aqueous Species Produced by the Dissolution of Calcite and LAWABP1 Glass Containing Trace Amounts of I, Tc, Se, U, and Pu in Deionized Water

Species	Mol.Wt.	Hard Core Diameter
AlO_2^-	58.98	4.0
$B(OH)_3(aq)$	61.83	3.0
Ca^{2+}	40.08	6.0
$CO_2(aq)$	44.01	3.0
CO_3^{2-}	60.01	5.0
CrO_4^{2-}	115.99	4.0
$Fe(OH)_3(aq)$	106.87	3.0
H_2O	18.01	-4.0
H^+	1.01	9.0
HCO_3^-	61.02	4.0
$HCrO_4^-$	117.00	4.0
$HSiO_3^-$	77.09	4.0
IO_3^-	126.90	3.0
K^+	39.10	3.0
La^{3+}	138.91	9.0
Mg^{2+}	24.31	8.0
Na^+	22.99	4.0
Ni++	58.69	4.5
$O_2(aq)$	32.00	3.0
OH^-	17.01	3.0
$PuO_2(CO_3)_3^{4-}$	456.03	4.0
SeO_4^{2-}	142.96	4.0
$SiO_2(aq)$	60.08	3.0
TcO_4^-	162.00	4.0
$Ti(OH)_4(aq)$	115.91	3.0
$UO_2(CO_3)_2^{2-}$	390.05	4.0
$UO_2(CO_3)_3^{4-}$	450.06	4.0
$UO_2(OH)_2(aq)$	304.04	3.0
Zn^{2+}	65.39	6.0
$Zr(OH)_4(aq)$	159.25	3.0

product to be produced by the private contractor, and adding calcite caused the software to load Ca species that might be important in a disposal system with a concrete vault, the list of aqueous species given in Table 4 is expected to be reasonably complete. However, for conducting actual disposal system simulations, a number of these species were excluded from the simulations because their concentration will be extremely small over the range of chemical conditions anticipated for the ILAW disposal system.

Gas Species

Gas species are compounds such as CO_2 and O_2 that make up the air phase in STORM simulations. For each gas species, the following data is needed:

- Molecular Weight
- Number of elements in gaseous species
- Stoichiometric coefficient of each element

Only CO_2 and O_2 are expected to significantly influence the chemical environment in the near and far field.

Solid Species

For each solid species, the following data is needed:

- Mass Density (g cm^{-3})
- Stoichiometric coefficient of each element

The simulation results presented in the following sections will reference two different ILAW glass compositions, which are provided in Table 5 for reference.

The mass density of both glasses was assumed to be 2.68 g cm^{-3}. The compositions of the materials making up the backfill, filler, Hanford soil, and degraded concrete used in the simulations are listed in Table 6. The mass density is obtained by dividing the molecular weight by the molar volume of the compound.

Secondary phases are solids that precipitate from a supersaturated aqueous solution. A list of potential secondary phases that form from long-term weathering experiments with LAWABP1 glass and from modeling the solution chemistry observed in experiments with the EQ3/6 code is provided by (McGrail et al. 2001). McGrail et al. (2001), eliminated a large number of phases from consideration because: 1) formation of the phase is kinetically prohibited at the disposal system temperature of 15°C, 2) selection of the phase would violate the Gibbs phase rule, 3) simulations show that allowing the phase to form is inconsistent with a large body of laboratory test data with borosilicate glasses, or 4) the phase is unstable over the range of chemical environments expected for the ILAW disposal system. The final phase assemblage used in STORM simulations (see Table 7) was further constrained because preliminary runs showed that the phase never formed or formed in such small amounts that the effects were insignificant. The composition of the secondary minerals used in the simulations is listed in Table 7. The mass density is obtained by dividing the molecular weight by the molar volume of the solid.

Equilibrium Reactions

For each equilibrium reaction, the following data is needed:

- Stoichiometric coefficient of each aqueous species in each reaction
- Equilibrium constant at a temperature of 15°C.

Table 5. Composition (Mole Fraction) of ILAW Glasses Used in Simulations

Element	LAWABP1	HLP-31
Al	1.36×10^{-1}	5.06×10^{-2}
B	1.84×10^{-1}	2.22×10^{-1}
Ca		1.15×10^{-4}
Cl	1.13×10^{-2}	5.82×10^{-3}
Cr	1.82×10^{-4}	7.64×10^{-4}
F	1.46×10^{-3}	3.39×10^{-4}
Fe	2.16×10^{-2}	2.71×10^{-2}
I	1.54×10^{-7}	1.66×10^{-7}
K	3.23×10^{-2}	6.44×10^{-3}
La	8.48×10^{-3}	
Mg	1.71×10^{-2}	1.47×10^{-2}
Na	4.46×10^{-1}	4.79×10^{-1}
O	1.87	1.87
P	7.79×10^{-4}	5.45×10^{-4}
Pu	3.52×10^{-8}	3.78×10^{-8}
Tc	6.59×10^{-7}	7.58×10^{-7}
S	8.63×10^{-4}	6.44×10^{-4}
Se	1.77×10^{-8}	1.90×10^{-8}
Si	4.82×10^{-1}	5.58×10^{-1}
Ti	2.15×10^{-2}	1.48×10^{-2}
U	9.81×10^{-5}	1.05×10^{-4}
Zn	2.20×10^{-2}	7.29×10^{-3}
Zr	2.94×10^{-2}	4.82×10^{-3}

Table 6. Composition of Native and Other Surrounding Materials Used in Simulations

Species	Formula	Mol.Wt.	Molar Volume
Albite	$NaAlSi_3O_8$	262.2	100.4
Illite	$K_{0.6}Mg_{0.25}Al_{1.8}Al_{0.5}Si_{3.5}O_{10}(OH)_2$	383.9	500.0
K-Feldspar	$KAlSi_3O_8$	278.3	108.8
Portlandite	$Ca(OH)_2$	74.0	500.0
Quartz	SiO_2	60.0	22.6

Table 7. Composition of Secondary Minerals Used in Simulations

Species	Formula	Mol.Wt.	Molar Volume
Amorphous silica	SiO_2	60.0	29.0
Analcime	$Na_{0.96}Al_{0.96}Si_{2.04}O_6$	201.2	89.1
Anatase	TiO_2	79.8	18.8
Baddeleyite	ZrO_2	123.2	21.9
Gibbsite	$Al(OH)_3$	78.0	31.9
Goethite	FeOOH	88.8	20.8
Herschelite	$Na_{1.62}K_{0.5}Al_{2.26}Si_4O_{12.45}{\cdot}6H_2O$	537.4	29.9
La(OH)3	$La(OH)_3$	189.9	54.5
Nontronite-Na	$Na_{0.33}Fe_2Al_{0.33}Si_{3.67}O_{11}{\cdot}H_2O$	425.2	184.8
PuO2	PuO_2	276.0	23.8
Sepiolite	$Mg_4Si_6O_{15}(OH)_2{:}6H_2O$	647.8	285.6
Soddyite	$(UO_2)2(SiO_4){:}2H_2O$	668.1	131.2
Theophrasite(1)	$Ni(OH)_2$	92.7	22.3
Weeksite	$K_2(UO_2)_2Si_6O_{15}{\cdot}4H_2O$	1098.8	500.0
Zn(OH)2	$Zn(OH)_2$	99.4	500.0

(1) Used in sensitivity case with steel container. See Section entitled "Surrounding Materials, Effect of Steel Container."

The equilibrium reactions in Table 8 were identified by simulating the dissolution of LAWABP1 glass in deionized water at 15°C with the EQ3/6 code package (Wolery and Daveler 1992) and the data0.com.R8 database (Daveler and Wolery 1992; Wolery and Daveler 1992). It was possible to exclude a significant number of secondary aqueous species from the simulations because their concentration was extremely small over the range of chemical conditions anticipated for the ILAW disposal system.

Table 8. Equilibrium Reactions From Dissolution of LAWABP1 Glass at 15°C

Reaction	Log K	Source
$CO_2(aq) + H_2O \rightleftharpoons H^+ + HCO_3^-$	-6.417	(Shock et al. 1989)
$CO_3^{2-} + H^+ \rightleftharpoons HCO_3^-$	10.429	(Shock and Helgeson 1988)
$HCrO_4^- \rightleftharpoons CrO_4^{2-} + H^+$	-6.491	(Shock and Helgeson 1988)
$HSiO_3^- + H^+ \rightleftharpoons SiO_2(aq) + H_2O$	10.101	(Sverjensky and Sahai 1996)
$OH^- + H^+ \rightleftharpoons H_2O$	14.344	(Shock and Helgeson 1988)
$UO_2(CO_3)_3^{4-} + 2H_2O + H^+ \rightleftharpoons 3HCO_3^- + UO_2(OH)2(aq)$	-0.970	(Grenthe et al. 1992)
$UO_2(CO_3)_2^{2-} + 2H_2O \rightleftharpoons 2HCO_3^- + UO_2(OH)2(aq)$	-6.520	(Grenthe et al. 1992)

Kinetic Reactions

For each kinetic reaction, the following data is needed:

- Mass action law type: {full = 1} {reduced = -1} {glass = 0}
- Stoichiometric coefficient of aqueous species in each reaction

- Equilibrium constant at a temperature of 15°C.
- Rate constant of reaction

A full mass action law type will be used for each solid phase except the waste glass. A special mass action law type implemented in the STORM code will be used for the glass, and will be discussed in the following section.

Compilations of kinetic rate constants, equivalent to thermodynamic databases for important mineral phases, are not available. Also, the available mineral dissolution/precipitation kinetics data are much more limited as compared with thermodynamic data. Consequently, sufficiently large rate constants will be used to approximate equilibrium conditions, i.e. ensure that the phase will precipitate rapidly if the local chemical environment at a grid node is saturated with respect to the particular phase. This has an additional advantage in that uncertainty in the exact value of a particular rate constant will have little impact on the calculations.

Glass Rate Law

The corrosion reaction for LAWABP1 glass used in the waste form release calculations is:

$$\begin{aligned}\text{LAWABP1} + 4.42\times10^{-1}\ \mathrm{H^+} + 1.89\times10^{-1}\ \mathrm{H_2O} \rightarrow\ & 1.36\times10^{-1}\ \mathrm{AlO_2^-} \\ & + 1.84\times10^{-1}\ \mathrm{B(OH)_3(aq)} + 1.13\times10^{-2}\ \mathrm{Cl^-} + 1.82\times10^{-4}\ \mathrm{CrO_4^{2-}} \\ & + 1.46\times10^{-3}\ \mathrm{F^-} + 2.16\times10^{-2}\ \mathrm{Fe(OH)_3(aq)} + 1.54\times10^{-7}\ \mathrm{IO_3^-} \\ & + 3.23\times10^{-2}\ \mathrm{K^+} + 8.48\times10^{-3}\ \mathrm{La^{3+}} + 1.71\times10^{-2}\ \mathrm{Mg^{2+}} + 4.46\times10^{-1}\ \mathrm{Na^+} \\ & + 7.79\times10^{-4}\ \mathrm{HPO_4^{2-}} + 3.52\times10^{-8}\ \mathrm{PuO_2(CO_3)_3^{4-}} + 8.63\times10^{-4}\ \mathrm{SO_4^{2-}} \\ & + 1.77\times10^{-8}\ \mathrm{SeO_4^{2-}} + 4.82\times10^{-1}\ \mathrm{SiO_2(aq)} + 6.59\times10^{-7}\ \mathrm{TcO_4^-} \\ & + 2.15\times10^{-2}\ \mathrm{Ti(OH)_4(aq)} + 9.81\times10^{-7}\ \mathrm{UO_2(OH)_2(aq)} \\ & + 2.20\times10^{-2}\ \mathrm{Zn^{2+}} + 2.94\times10^{-2}\ \mathrm{Zr(OH)_4(aq)}\end{aligned} \quad (1)$$

Similarly, the corrosion reaction for HLP-31 glass is

$$\begin{aligned}\text{HLP-31} \rightarrow\ & 6.84\times10^{-1}\ \mathrm{OH^-} + 5.06\times10^{-2}\ \mathrm{Al^{3+}} + 2.22\times10^{-1}\ \mathrm{B(OH)_3(aq)} \\ & + 1.15\times10^{-4}\ \mathrm{Ca^{2+}} + 7.64\times10^{-4}\ \mathrm{CrO_4^{2-}} + 2.72\times10^{-2}\ \mathrm{Fe(OH)_3(aq)} \\ & + 1.66\times10^{-7}\ \mathrm{IO_3^-} + 6.44\times10^{-3}\ \mathrm{K^+} + 1.47\times10^{-2}\ \mathrm{Mg^{2+}} + 4.78\times10^{-1}\ \mathrm{Na^+} \\ & + 3.78\times10^{-8}\ \mathrm{PuO_2(CO_3)_3^{4-}} + 1.90\times10^{-8}\ \mathrm{SeO_4^{2-}} + 5.58\times10^{-1}\ \mathrm{SiO_2(aq)} \\ & + 7.58\times10^{-7}\ \mathrm{TcO_4^-} + 1.48\times10^{-2}\ \mathrm{Ti(OH)_4(aq)} + 1.05\times10^{-4}\ \mathrm{UO_2(OH)_2(aq)} \\ & + 7.29\times10^{-3}\ \mathrm{Zn^{2+}} + 4.82\times10^{-3}\ \mathrm{Zr(OH)_4(aq)}\end{aligned} \quad (2)$$

The stoichiometric coefficients for the radionuclides I, Pu, Se, and Tc are based on the average package concentration from the *Immobilized Low Activity Tank Waste Inventory Data Package* (Wootan 1999). For a dissolution reaction involving glass, parameters associated with the following kinetic rate law are needed

$$r_g = \vec{k} a_{H^+}^{-\eta} e^{\frac{-E_a}{RT}} \left[1 - \left(\frac{Q}{K_g} \right)^{\sigma} \right] \quad (3)$$

where r_g = dissolution rate, g m^{-2} d^{-1}
$\vec{k}$ = intrinsic rate constant, g m^{-2} d^{-1}
a_{H^+} = hydrogen ion activity (variable to be calculated by STORM)
E_a = activation energy, kJ/mol
R = gas constant, kJ/(mol·K)
T = temperature, K (assumed constant at 15°C)
Q = ion activity product Glass(variable to be calculated by STORM)
K_g = pseudoequilibrium constant
η = pH power law coefficient
σ = Temkin coefficient (σ = 1 assumed).

Equation (3) is an approximation for glass because glass is metastable, and the reaction proceeds one way (i.e., glass dissolves). The unknown parameters in Equation (1) ($\vec{k}$, E_a, K_g, and η) have been determined for LAWABP1 and HLP-31 (McGrail et al. 2001) glasses and these values are given in Table 9. The values given by McGrail et al. (2001) for LAWABP1 glass differ slightly with respect to the values given in Table 9, which were based on an earlier revision of the Waste Form Release Data Package (McGrail et al. 2000). Additional data were developed between the time the STORM calculations were performed and when the data package was updated that changed the parameters slightly.

Test results with HLP-31 glass showed that unlike most silicate glasses, the dissolution rate did not diminish with increasing concentration of Si in solution. Consequently, no pseudoequilibrium phase or K_g was assigned to this glass. In addition, test results with LAWABP1 glass (and most other ILAW glasses) show that it is susceptible to a secondary reaction mechanism, alkali ion exchange. This reaction results in the selective extraction of Na via a reaction

$$\text{LAWABP1-Na} + H^+ \rightarrow \text{LAWABP1-H} + Na^+ \quad (4)$$

where LAWABP1-Na represents the unreacted glass containing Na and LAWABP1-H represents a hydrated glass where the Na has been replaced with an equimolar amount of hydrogen. The rate of this reaction has been determined from single-pass flow-through experiments by (McGrail et al. 2001) and the rate constant is 2.5 x 10^6 g m^{-2} s^{-1} (again, slightly different from the value given in Table 9). STORM keeps track of the amount of hydrated glass formed via Reaction (4) and then allows it to dissolve

according to the same kinetic rate law (3) as the parent glass. The ion-exchange rate for HLP-31 glass was set at zero, consistent with the results reported by (McGrail et al. 2001).

Secondary Phase Equilibrium Constants

McGrail et al. (2001) describe the methods used to develop a solubility product for the key secondary phases identified from laboratory testing and from simulations with the EQ3/6 code. For convenience, the log K they derived for each secondary phase given in Table 7 is reproduced in Table 10. For the secondary phases where a log K was not available or could not be estimated, the reaction was not included in the STORM simulations.

Table 9. Summary of Kinetic Rate Parameters Used for Glasses

Parameter	Meaning	LAWABP1	HLP-31	Comment
$\vec{k}$	Intrinsic rate constant	3.5×10^{5} g m^{-2} d^{-1}	3 x 10^{6} g m^{-2} d^{-1}	HLP-31 assumed roughly 10 times faster than LAWABP1
K_g	Apparent equilibrium constant for glass based on activity of SiO_2(aq)	$10^{-2.9}$	N/A	HLP-31 glass dissolution rate did not change as a function of SiO_2(aq)
η	pH power law coefficient	0.5	0.5	HLP-31 value assumed same as LAWABP1
E_a	Activation energy of glass dissolution reaction	75 kJ/mol	75 kJ/mol	HLP-31 value assumed same as LAWABP1
σ	Temkin coefficient	1	1	Assigned constant
r_x	Na ion-exchange rate	3.5×10^{-6} mol m^{-2} d^{-1}	0	No detectable ion exchange for HLP-31

Initial and Boundary Conditions

For each specified gas species concentration, the following data are needed:

- Partial pressure of gaseous species

The gas partial pressure for CO_2 and O_2 were fixed at atmospheric values of $3x10^{-4}$ and $2.1x10^{-1}$ atm, respectively.

Table 10. Secondary Phase Reaction Network for LAWABP1 Glass

Reaction	Log K (15°C)
$Al(OH)_3(am) \rightleftharpoons AlO_2^- + H^+ + H_2O$	-13.10
$Analcime \rightleftharpoons 0.96AlO_2^- + 0.96Na^+ + 2.04SiO_2(aq)$	-9.86
$Anatase + 2H_2O \rightleftharpoons Ti(OH)_4(aq)$	-6.64
$Baddeleyite + 2H_2O \rightleftharpoons Zr(OH)_4(aq)$	-9.29
$Goethite + H_2O \rightleftharpoons Fe(OH)_3(aq)$	-11.09
$Herschelite \rightleftharpoons 1.62Na^+ (aq) + 0.50K^+ (aq) + 2.26AlO_2^- + 4SiO_2(aq) + 0.14H^+ + 5.93H_2O$	-40.94
$La(OH)_3(am) + 3H^+ \rightleftharpoons 3H_2O + La^{3+}$	22.55
$Nontronite\text{-}Na + 2H_2O \rightleftharpoons 0.330AlO_2^- + 2Fe(OH)_3(aq) + 0.330Na^+ + 3.67SiO_2(aq)$	-43.33
$PuO_2 + HCO_3^- + 0.5O_2(aq) \rightleftharpoons PuO_2(CO_3)_3^{4-} + H_2O + H^+$	-15.92
$Sepiolite + 8H^+ \rightleftharpoons 4Mg^{2+} + 6SiO_2(aq) + 11H_2O$	31.29
$SiO_2(am) \rightleftharpoons SiO_2(aq)$	-2.85
$Weeksite + 2H^+ \rightleftharpoons 2K^+ + 2\ UO_2(OH)_2(aq) + 6SiO_2(aq) + 3H_2O$	-5.25
$Soddyite \rightleftharpoons 2UO_2(OH)_2(aq) + SiO_2(aq)$	-20.24
$Theophrasite + 2H^+ \rightleftharpoons 2H_2O + Ni^{2+}$	13.33
$Zn(OH)_2(am) + 2H^+ \rightleftharpoons 2H_2O + Zn^{2+}$	14.44

For each specified aqueous species, the following data are needed:

- Specified total concentration
- Stoichiometric coefficient of each aqueous species.

Aqueous species concentrations at the upper boundary, and for initial conditions, were specified as a part of the near-field geochemistry data package (Kaplan and Serne 1999) and are given in Table 11.

For water flow the following boundary conditions were used: constant specified flux at the upper boundary and free drainage at the lower boundary. The reactive transport simulations used the following boundary conditions: specified aqueous species concentrations at the upper boundary and no diffusion across the lower boundary. The contaminant flux across the lower boundary is therefore limited to advection

$$f = c\rho_w v \tag{5}$$

where c = concentration (mol kg^{-1})
ρ_w = density of water (kg m^{-3})
v = specific discharge (m s^{-1})

Table 11. Initial Aqueous Concentrations Used in Simulations

Species	Initial Concentration (mol kg-1)
AlO_2^-	10^{-6}
$B(OH)_3(aq)$	10^{-10}
Ca^{2+}	10^{-7}
Cr (total)	10^{-10}
$Fe(OH)_3(aq)$	10^{-10}
H_2O	1
H^+	10^{-7}
IO_3^-	10^{-10}
K^+	10^{-6}
La^{3+}	10^{-10}
Mg^{2+}	10^{-10}
Na^+	10^{-6}
Ni^{2+}	10^{-10}
$PuO_2(CO_3)_3^{4-}$	10^{-10}
SeO_4^{2-}	10^{-10}
Si (total)	10^{-5}
TcO_4^-	10^{-10}
$Ti(OH)_4(aq)$	10^{-10}
U (total)	10^{-10}
Zn^{2+}	10^{-10}
$Zr(OH)_4(aq)$	10^{-10}

Model Output

The normalized flux to the vadose zone is calculated by summing the flux at each node across the bottom boundary of the model, and normalizing the total flux according to the amount of each radionuclide in all the waste packages at the start of the simulation. The normalized flux across the lower boundary, *F*, in units of ppm/yr, was calculated using

$$F = \frac{\sum_{i=1}^{N} f_i \Delta x_i \Delta y_i}{I_j} (3.1558 \times 10^7 \text{ s yr}^{-1})(1 \times 10^6 \text{ ppm}) \quad (6)$$

where f_i = flux across the bottom of an individual grid block (μmole m^{-2} s^{-1})

$\Delta x_i \Delta y_i$ = cross-sectional area of an individual grid block (m^2)

I_j = inventory of *j*th radionuclide in the waste packages (μmol), where

$$I_j = V_{wp} (1 - \theta_T) V_G \rho_G \gamma_j \quad (7)$$

where V_{wp} = volume of the waste packages (m^3)

θ_T = total porosity of the material representing the waste packages (0.02)

V_G = fraction of glass in each waste package (0.85)

ρ_G = molar density of LAWABP1 glass (38776.1450 moles m^{-3})

γ_j = mole fraction of *j*th radionuclide in LAWABP1 glass (i.e., 6.59×10^{-1} μmoles Tc $mole^{-1}$ glass)

The volume of the waste packages, V_{wp}, was 5.6 m^3 for the RH Trench simulations and 8.4 m^3 for the new ILAW concrete vault simulations. For 1-D simulations, the cross-sectional area of the grid block was 1 m^2.

Results

A total of 22 simulations were run to test the sensitivity of model calculations to various assumptions (Table 12). Discussion of the results of each simulation is contained in the following sections.

Table 12. List of Waste Form Sensitivity Cases

Case	Description	Basic Model
WFA	4.2 mm/yr infiltration	Trench
WFB	Forward rate, 4.2 mm/yr infiltration	Trench
WFC	4.2 mm/yr infiltration	Vault
WFD	0.1 mm/yr infiltration	Trench
WF1	Assume no Ion Exchange	Trench
WF2	Assume no Secondary Phase Formation	Trench
WF4	0.9 mm/yr infiltration rate	Trench
WF6	50 mm/yr infiltration rate	Trench
WF7	0.5 mm/yr infiltration rate	Trench
WF8	10 mm/yr infiltration rate	Trench
WF9	Extend WFA to groundwater	Trench
WF10	Add conditioning layer at top	Trench
WF11	Change filler material in trench to sand	Trench
WF14	Increase diffusion for all aqueous species by a factor of 10	Trench
WF16	Replace concrete everywhere with backfill material	Vault
WF19	0.9 mm/yr infiltration rate	Vault
WF21	0.1 mm/yr infiltration	Vault
WF25	Include steel in waste packages	Trench
WF26	Replace Tc w/U	Trench
WF27	Full 2-D simulation	Trench
WF28/WFx	Increase Waste Loading / Alternate Glass Formulation (HLP-31)	Trench
WF30	Increase ion exchange rate by 5 times for WFB	Trench

Base Case

The maximum flux of Tc to the vadose zone for the RH Trench base case simulation is 0.93 ppm/yr at 100,000 yr as shown in Figure 3. The Tc flux to the vadose zone is proportional to the TcO_4^- concentration at the lower boundary and the water flux rate. At early times, the TcO_4^- concentrations (Figure 4) increase sharply in the glass layers. Glass dissolution, and low water contents in the glass layers, coupled with a low water flux rate, causes TcO_4^- concentrations to increase rapidly in the glass layers. In contrast, mass transport from the glass layers is required to build up Tc concentrations in the backfill layers. Therefore, concentrations in the backfill layers increase slowly as products of glass dissolution diffuse from the glass layers into the backfill layers, where dilution also occurs because of the

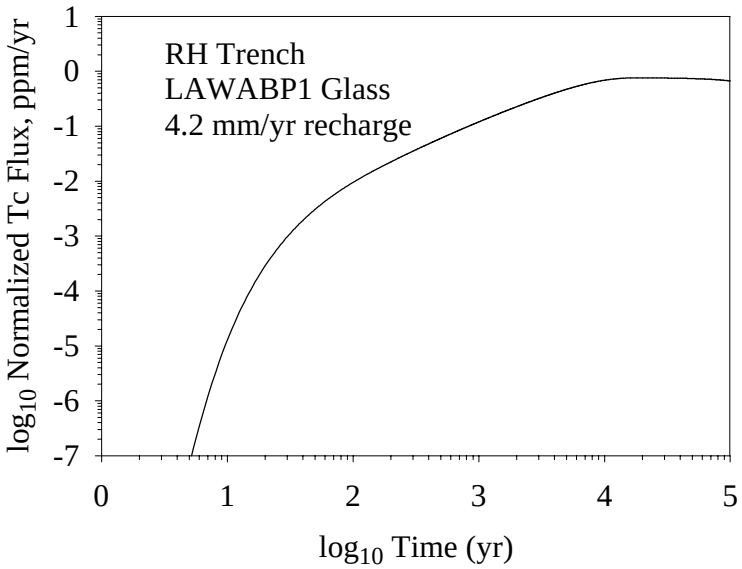

Figure 3. Tc Flux to the Vadose Zone, Corrected for Radioactive Decay, Normalized to the Amount of Tc Originally in LAWABP1 Waste Glass, for Base Case Trench Simulation

much higher water content in the backfill layers compared with the glass layers. Predicted glass dissolution rates (Figure 5) increase with time in each of the glass layers, but are relatively similar for each layer. The pH and TcO_4^- concentrations increase more rapidly in the glass layers early in the simulation, although by 20,000 yr, concentrations throughout the profile are relatively similar. This indicates that at early times, the TcO_4^- flux across the lower boundary is limited by the diffusion rate of TcO_4^- out of the glass layers.

The glass dissolution rate for these simulations is highest on the edges of the glass layers. This is where the pH of the pore water is highest (Figure 6) and the SiO_2(aq) concentrations are lowest (Figure 7). Concentration of SiO_2(aq) is lower in the backfill due to precipitation of quartz, one of the primary minerals that make up the backfill. As was mentioned in the Methods Section, dissolution/precipitation rate constants for each mineral were set to relative high values to approximate equilibrium conditions in the simulations. However, quartz precipitation is extremely slow at the disposal system temperature (15°C) and would not be expected to precipitate in significant amounts. Future simulations will correct this, but by enforcing equilibrium with quartz, the present calculations are conservative as the effect is to increase the calculated glass dissolution rates at the glass/backfill interface.

Because the glass dissolution rate is relatively low, the surface area of the glass does not decrease noticeably by 20,000 yr. Similarly, the volume of secondary minerals precipitated is also low (Figure 8).

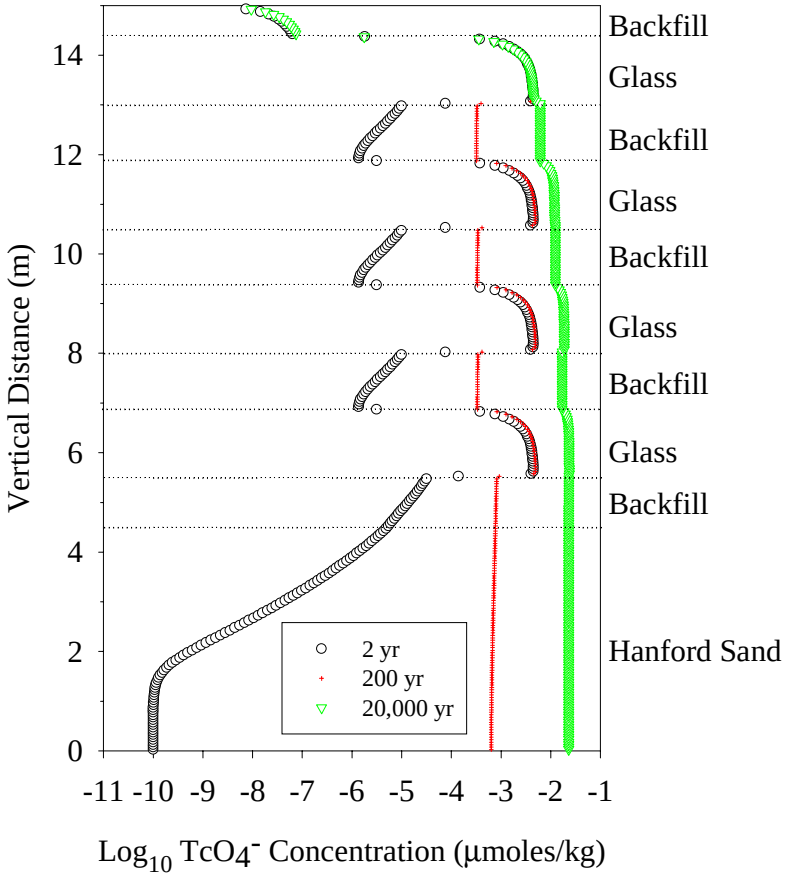

Figure 4. TcO_4^- Concentrations for RH Trench Simulation with Recharge Rate of 4.2 mm/yr (Horizontal Dotted Lines Represent Boundaries Between Material Zones and Material Names Are Shown Along Right Axis)

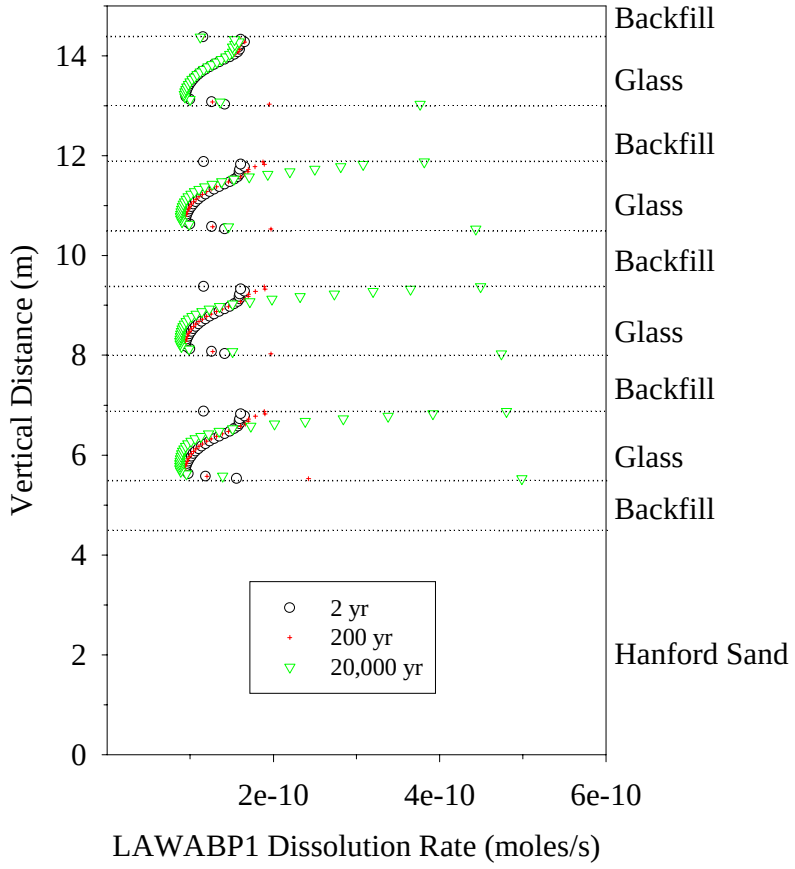

Figure 5. Glass Dissolution Rate for LAWABP1 in RH Trench Simulation with Recharge Rate of 4.2 mm/yr (horizontal dotted lines represent boundaries between material zones and material names are shown along right axis)

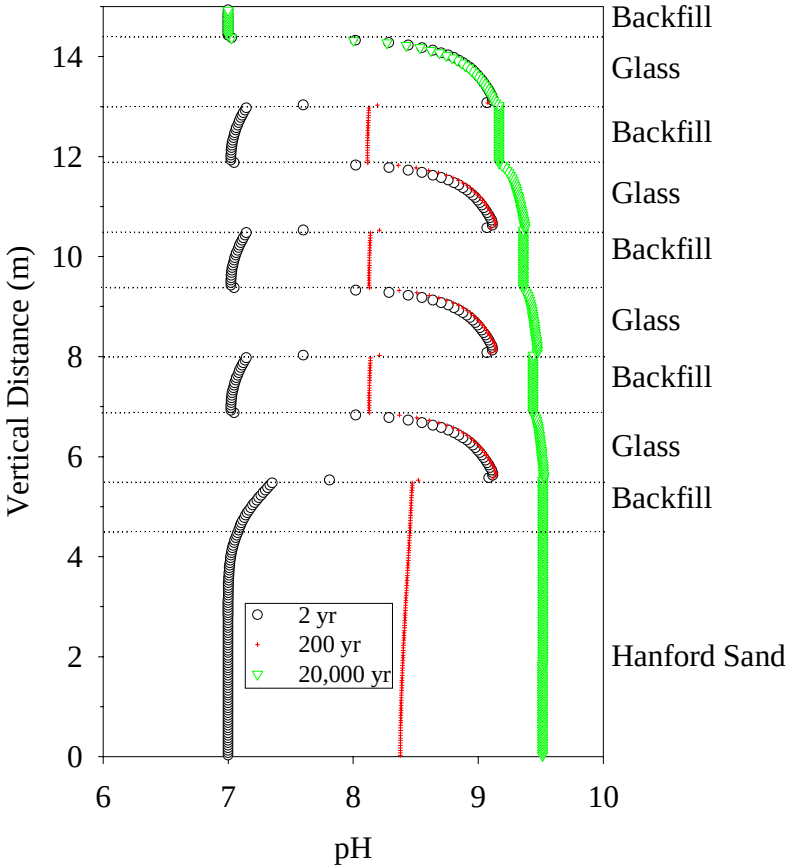

Figure 6. Solution pH for RH Trench Simulation with Recharge Rate of 4.2 mm/yr (horizontal dotted lines represent boundaries between material zonesand material names are shown along right axis)

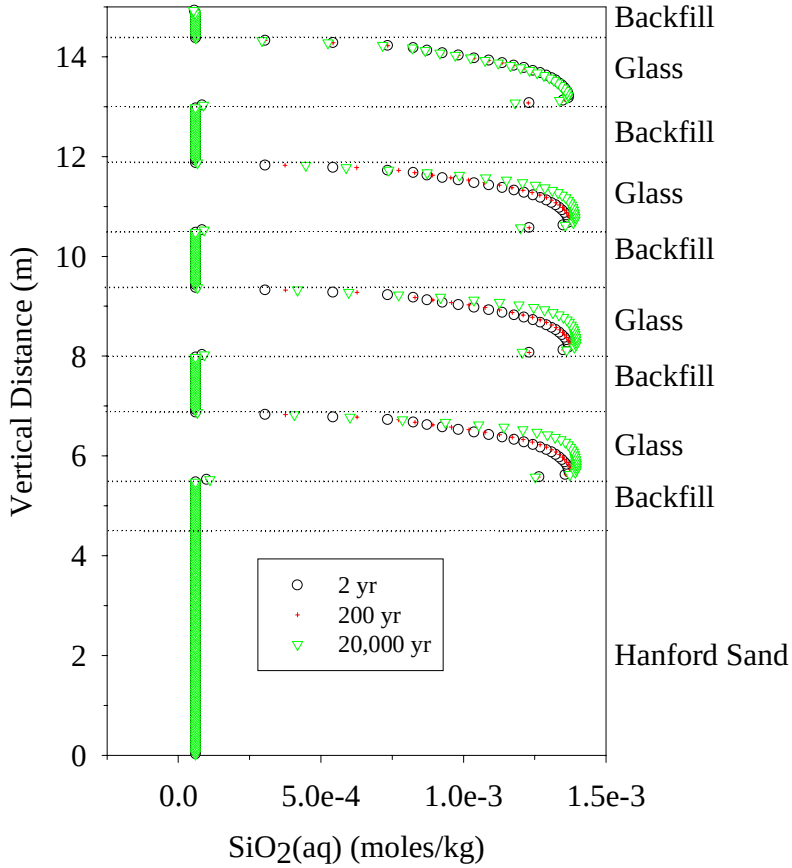

Figure 7. SiO_2(aq) Concentrations for RH Trench Simulation with Recharge Rate of 4.2 mm/yr (horizontal dotted lines represent boundaries between material zones and material names are shown along right axis)

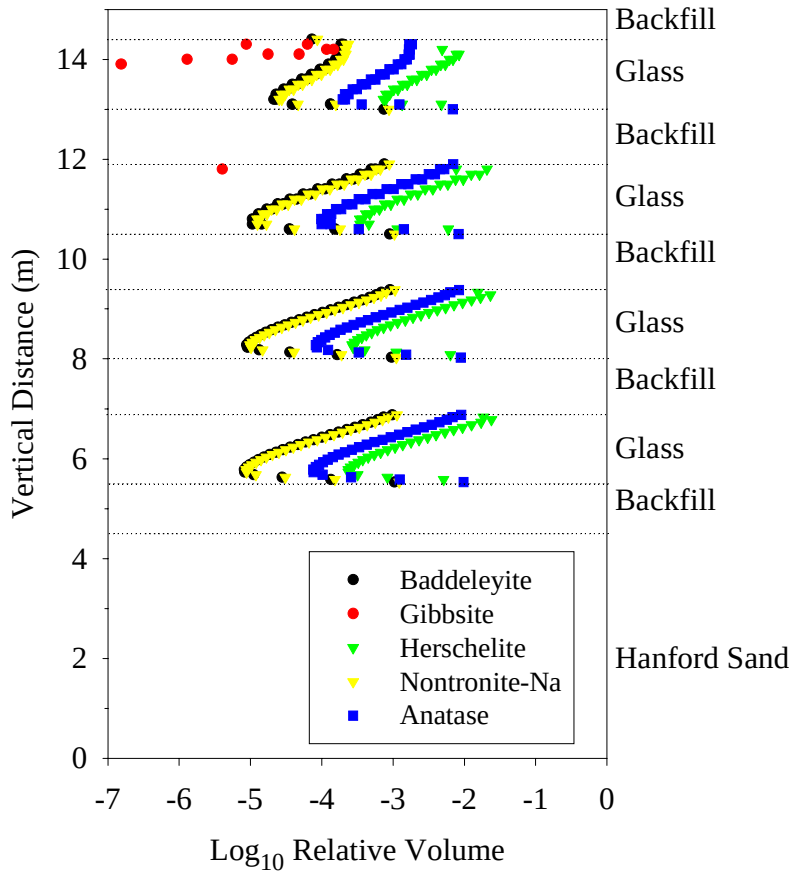

Figure 8. Secondary Mineral Relative Volumes at 20,000 yr for RH Trench Simulation with Recharge Rate of 4.2 mm/yr (horizontal dotted lines represent boundaries between material zones and material names are shown along right axis)

Other Radionuclide Release Rates

The base case simulation was modified to consider the release of uranium species from the waste glass. Three aqueous uranium species were considered: $UO_2(CO_3)_2^{2-}$, $UO_2(CO_3)_3^{4-}$, and $UO_2(OH)_2(aq)$. Two secondary minerals were considered: Weeksite, $K_2(UO_2)_2Si_6O_{15}{\cdot}4H_2O$, and soddyite, $(UO_2)_2(SiO_4){\cdot}2H_2O$. Only soddyite precipitated, in miniscule amounts, and for a very short period. Because of the slow release rate from the glass, steady rate of mass transport through the system, and strong carbonate complexes associated with U(VI), the pore fluid remained undersaturated with respect to weeksite and soddyite and the uranium remained dissolved in the aqueous phase. Hence, the normalized fluxes for total U release are identical to those predicted for Tc.

Because no solid phases were identified that could limit Se and I solubility, their release rates were determined by the rate of glass dissolution, normalized by their inventory. Hence, the normalized fluxes for Se and I are also identical to those predicted for Tc. In contrast, Pu release is controlled by the solubility of PuO_2 (Table 10) with the major aqueous species being $PuO_2(CO_3)_3^{4-}$. Therefore, the normalized flux for Pu is several orders of magnitude lower than that for Tc as shown in Figure 9.

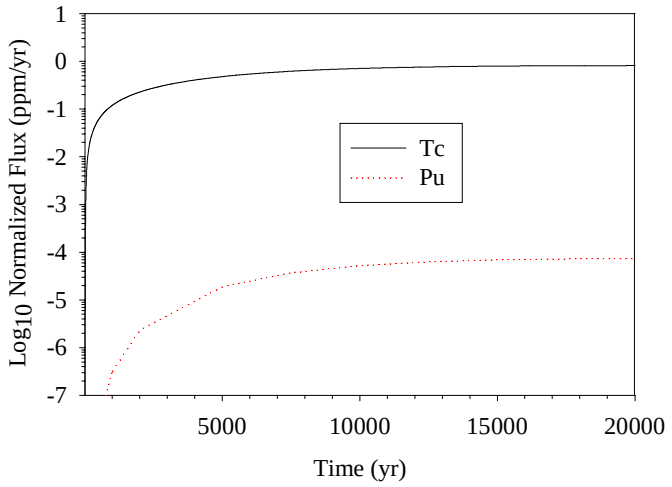

Figure 9. Comparison of Pu and Tc Flux to the Vadose Zone for Base Case Trench Simulation

Recharge Rates

Assuming steady-state flow with a constant recharge rate results in a constant water flux, equal to the recharge rate, throughout the entire depth of the profile. Water content, however, will vary with depth in the profile. Water content is a dimensionless variable defined as the volume of water per volume of porous or fractured media. The unique relationship between water flux and water content for each material is defined by the hydraulic parameters (Meyer and Serne 1999).

The flux of ^{99}Tc increases with increasing recharge rate (Figure 10). Higher recharge rates flush dilute water through the system, increasing water contents in the glass layers (Figure 11), lowering the $SiO_2(aq)$ concentration, thus increasing the glass dissolution rate. However, the diluting effect of higher recharge also limits increases in pH, thereby limiting increases in the glass dissolution rate.

Glass Dissolution Model

The effect of the assumptions inherent in the glass dissolution model was also considered. A comparison of the base case with a simulation at the forward rate of reaction is shown in Figure 12. At the forward rate of reaction, buildup in the activities of species caused by glass dissolution, such as AlO_2^- and $SiO_2(aq)$, is not considered to decrease the glass dissolution rate. In this case, Equation (3) simplifies to

$$r_g = \bar{k} a_{H^+}^{-\eta} e \frac{-E_a}{RT} \quad (8)$$

so that only solution pH affects the dissolution rate (temperature is constant at 15°C). Allowing the glass dissolution rate to decrease as the concentration of SiO_2(aq) increases lowers the relative flux of Tc to the vadose zone by a factor of 8 as compared with the case with glass dissolving at the forward rate, as shown in Figure 12.

If no ion exchange is assumed, the glass dissolution rate decreases slightly from the lower pH. If no secondary mineral precipitation is allowed, the amount of SiO_2(aq) in solution is greater, thus lowering the dissolution rate further relative to the forward rate. If, for the forward rte simulation, the ion exchange rate is increased by a factor of five, the overall glass dissolution rate increases only slightly. The strong buffering effect of dissolution of CO_2(g) to produce carbonic acid prevents the increased ion-exchange rate from affecting the pH significantly.

Surrounding Materials

Preconditioning Layer

Placing a 1-m thick layer of silica sand on the top of the trench lowers the glass dissolution rate very slightly by increasing the amount of silica in solution (Figure 13). The effect is small because the high solid to liquid ratio associated with the glass dominates the solution chemistry after only a short

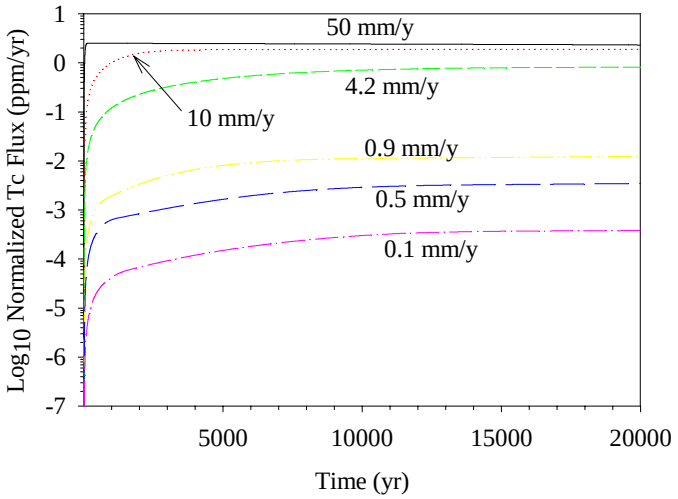

Figure 10. Flux of ^{99}Tc to the Vadose Zone, Relative to the Amount of Tc Originally in LAWABP1 Waste Glass, for Recharge Rates Ranging from 0.1 to 50 mm/yr

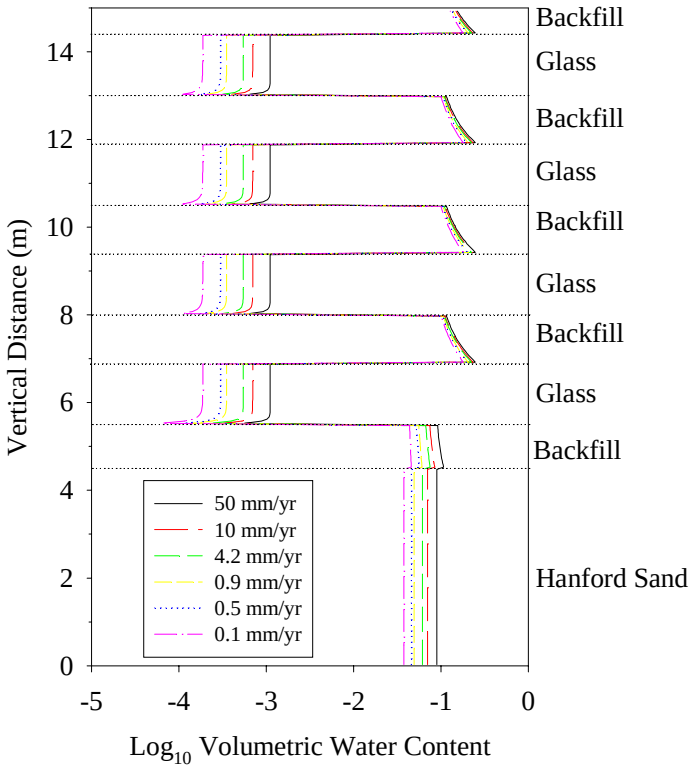

Figure 11. Water Content vs. Depth for Selected Recharge Rates for the RH Trench

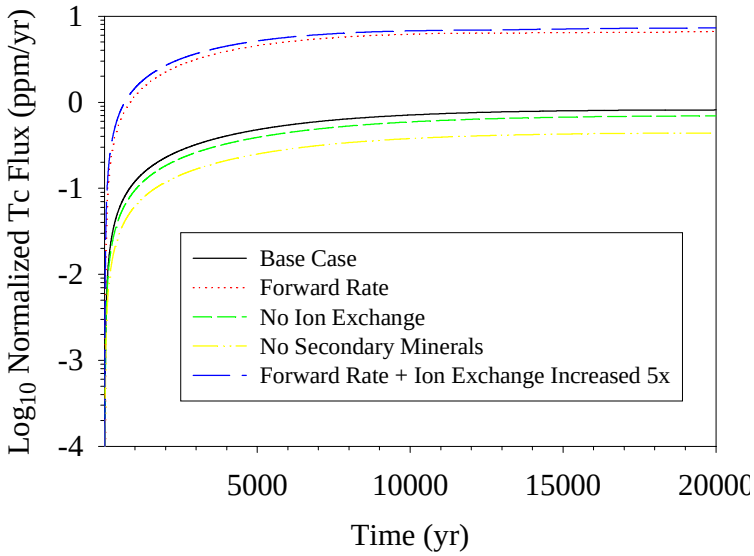

Figure 12. Tc Flux to the Vadose Zone, Relative to the Amount of Tc Originally in LAWABP1 Waste Glass, for Different Glass Dissolution Models

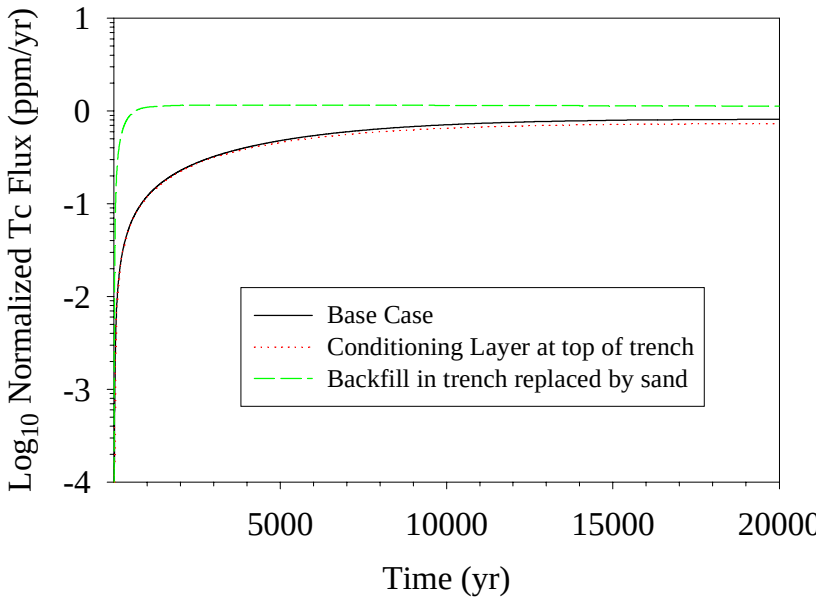

Figure 13. Tc Flux to the Vadose Zone, Relative to the Amount of Tc Originally in LAWABP1 Waste Glass, Assuming Different Surrounding Materials

penetration depth into the first layer of waste packages. Hence, the silica-sand layer only affects a small volume of glass right at the silica-sand/glass interface. Replacing the backfill material in the trench with sand (hydraulic properties only were changed to those of the Vault Filler material) causes an increase in the release rate. The sand has lower moisture content and thus, a higher linear pore velocity than the backfill at a recharge of 4.2 mm/y. This allows more rapid transport of Tc to the bottom of the facility.

Effect of Steel Container

Two sensitivity cases considered the effect of including the 304L stainless steel containers in which the molten LAW is poured. The corrosion reaction for 304 stainless steel is (Cloke et al. 1997):

$$\begin{aligned} \text{Steel} + 2.9262\times10^{-2}\ H^{+} + 1.7618\ H_2O + 3.4169\times10^{-1}\ O_2(aq) \rightarrow \\ 3.4667\times10^{-3}\ HCO_3^{-} + 3.4701\times10^{-1}\ CrO_4^{2-} + 1.1828\ Fe(OH)_3(aq) \\ + 3.5167\times10^{-2}\ Mn^{2+} + 9.9093\times10^{-3}\ NO_3^{-} + 1.8583\times10^{-1}\ Ni^{2+} \\ + 8.8004\times10^{-4}\ HPO_4^{2-} + 5.2008\times10^{-4}\ SO_4^{2-} + 1.7325\times10^{-2}\ SiO_2(aq) \end{aligned} \quad (9)$$

The 304L stainless steel corrosion rate was assumed to be a constant $6.87\text{x}10^{-14}$ mol cm^{-2} s^{-1} (Cloke et al. 1997). Thus, the steel corrosion rate is not affected by changes in pH or water chemistry. By assuming this rate, the stainless steel corrodes away entirely within 1,000 yr. For the first sensitivity case, stainless steel was included in the upper and lower nodes of each glass waste package layer.

Including the stainless steel waste containers increases the pH slightly, because the corrosion reaction consumes H^+, but the effect on the glass dissolution rate is negligible (Figure 15). However, 304L contains approximately 20% Cr and 10% Ni. The estimated inventory of chromium in the 304L is approximately 9.3×10^6 kg. In contrast, the ILAW glass contains only about 7×10^4 kg of Cr. As mentioned previously, using the assumed steel corrosion rate establishes a release time of approximately 1000 y. The short release time combined with the larger inventory of Cr in the steel combine to produce a much higher calculated release rate of Cr from the disposal system (Figure 14).

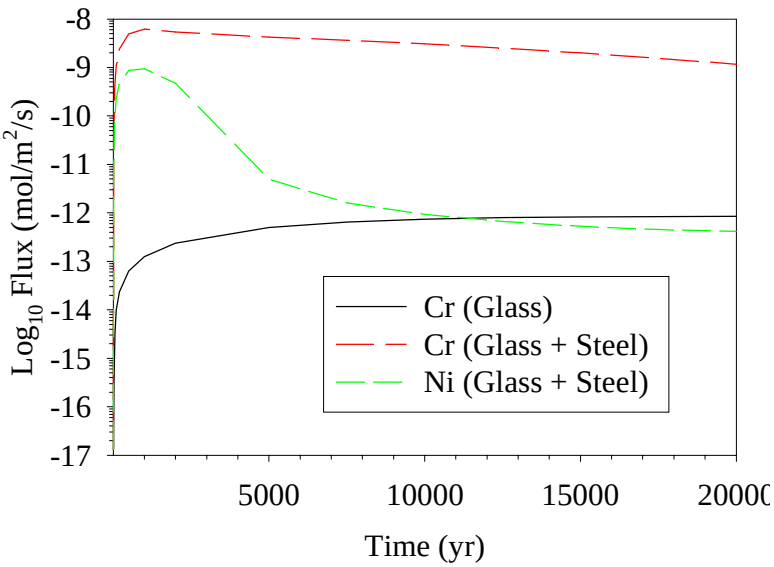

Figure 14. Tc Flux to the Vadose Zone, Relative to the Amount of Tc Originally in LAWABP1 Waste Glass, Including Stainless Steel Waste Packages

Because we have assumed global equilibrium with the atmosphere at all times, the Cr is released as soluble and mobile CrO_4^{2-}. The simulations do not account for the likely slow kinetics associated with oxidation of Cr(III) to Cr(VI) and thus represent the most conservative release case. The EQ3/6 database we have used has only a few solid alkali chromates, all of which are very soluble. A solubility product for $MgCrO_4$ and $CaCrO_4$ is available in the MINTEQA2 database. However, independent calculations using the listed log Ks and the composition of fluids exiting the LAW disposal show that these phases are several orders of magnitude undersaturated. So, no solid phase precipitated in our simulations that would limit the Cr release from the disposal system.

In contrast, the release rate of Ni is many times lower than that for Cr (Figure 14). Nickel release rate is constrained by precipitation of theophrasite, $Ni(OH)_2$. Because the solubility of theophrastite decreases with the square of the OH^- activity, the calculated release rate decreases markedly at later times as the pH increases throughout the disposal system.

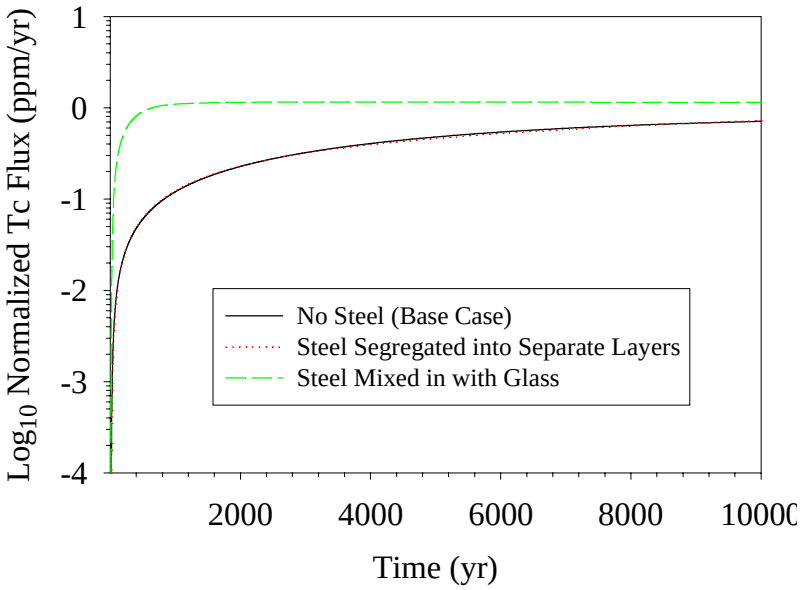

Figure 15. Tc Flux to the Vadose Zone, Relative to the Amount of Tc Originally in LAWABP1 Waste Glass, Including Stainless Steel Waste Packages

In a separate sensitivity case, the stainless steel was mixed uniformly throughout the entire glass layer. In this case, the steel corrosion reaction causes enhanced precipitation of nontronite, which lowers the activity of SiO_2(aq), and gives a 10-fold increase in the glass dissolution rate during the first few thousand years (the steel is completely dissolved after 1,000 yr so the effect is transient). This sensitivity case approximates batch (closed-system) laboratory experiments where glass and steel have been reacted together (Jantzen 1984; McGrail 1986). In these experiments, the presence of iron was found to significantly enhance glass dissolution rates because the steel corrosion products adsorbed Si or caused precipitation of ferrous silicate clay that acted as a sink for Si. Although these experimental findings are incontrovertible, assuming direct translation of the effects to an open disposal system is not correct. As the STORM simulations show, segregation of the stainless steel into layers, which is the more realistic case, had essentially no impact on glass performance. This is because Fe(III) is extremely insoluble and so the mass transported into the glass layers in very small. Consequently, the steel layers affect only a very small volume of glass near the steel/glass interface. In contrast, the homogeneous mixing of the steel with the glass impacts the entire volume within each glass layer. The large difference in results between these two scenarios emphasizes the importance of modeling the disposal system as realistically as possible and suggests caution when generalizing experimental results (particularly from batch experiments) to an open system.

Aqueous Diffusion Coefficient

Increasing the aqueous diffusion coefficient for all species to $5x10^{-8}$ m^2/s from a base case value of $5x10^{-9}$ m^2/s lowers the Tc flux to the vadose zone. The increased diffusion coefficient significantly

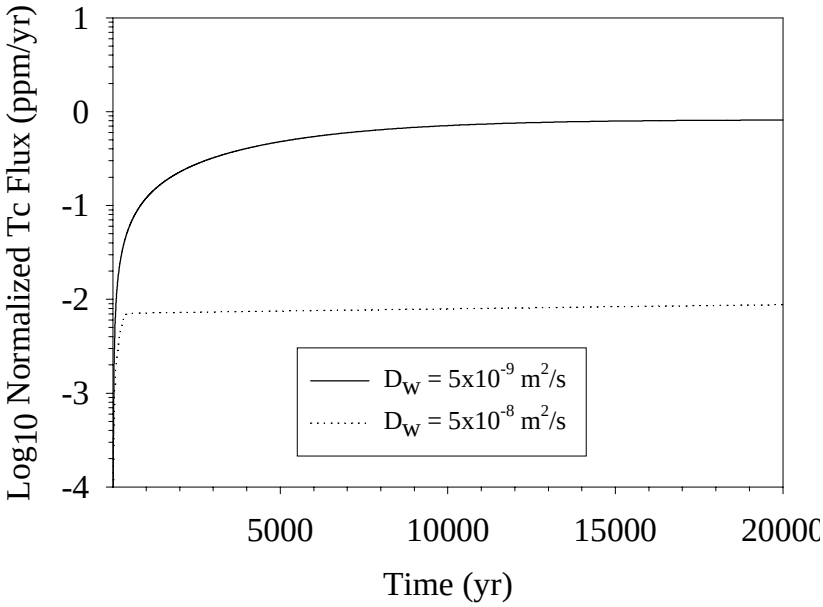

Figure 16. Tc Flux to the Vadose Zone, Relative to the Amount of Tc Originally in LAWABP1 Waste Glass, Assuming Different Aqueous Diffusion Coefficients

increases mixing of the aqueous products of glass dissolution into the backfill layers, the minerals in which act as a pH buffer. This results in a significantly lower pH in the glass layers, and hence a much lower glass dissolution rate (Figure 16).

Two-Dimensional Simulation

A full 2-D simulation of the trench scenario was developed for comparison to the 1-D simulation used as the base case. The 2-D simulation reaches steady state earlier and shows a lower normalized Tc release rate than the 1-D simulation (Figure 17). In the 2-D simulations, water flows around the glass waste packages. This lowers the water content (Figure 18) in, and water flux through, the waste packages, and increases the Tc concentrations (Figure 19) in the waste packages. The glass dissolution rate (Figure 20) for these simulations is highest on the edges of the glass layers. This is where the pH of the pore water is highest (Figure 21) and the SiO_2(aq) concentrations are lowest (Figure 22). Again, this is a consequence of quartz precipitation in the backfill.

This 2-D simulation required over a month to reach a simulation time of 2,000 yr, whereas the 1-D simulation required only 5.3 days to reach a simulation time of 100,000 yr. The results of this comparison show that the 1-D simulations are conservative with respect to the results from the 2-D simulations.

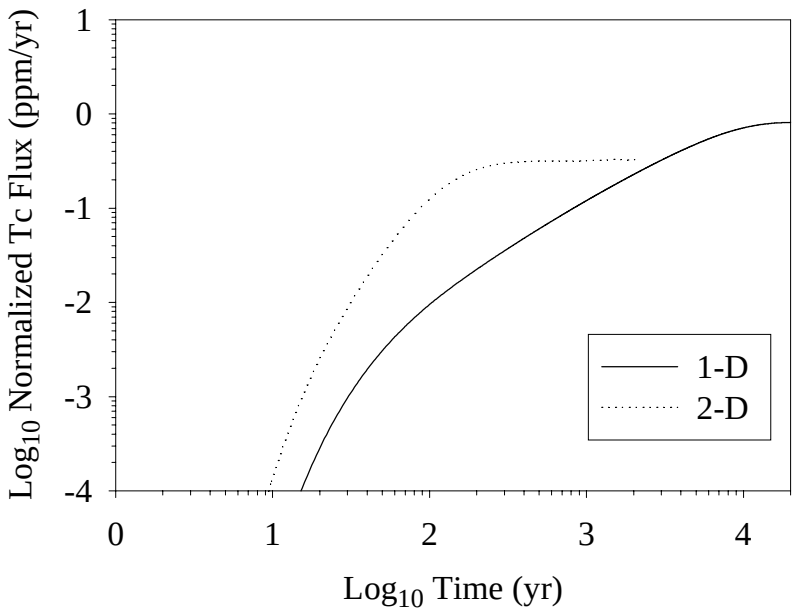

Figure 17. Tc Flux to the Vadose Zone, Relative to the Amount of Tc Originally in LAWABP1 Waste Glass, Comparing 1-D and 2-D Simulations

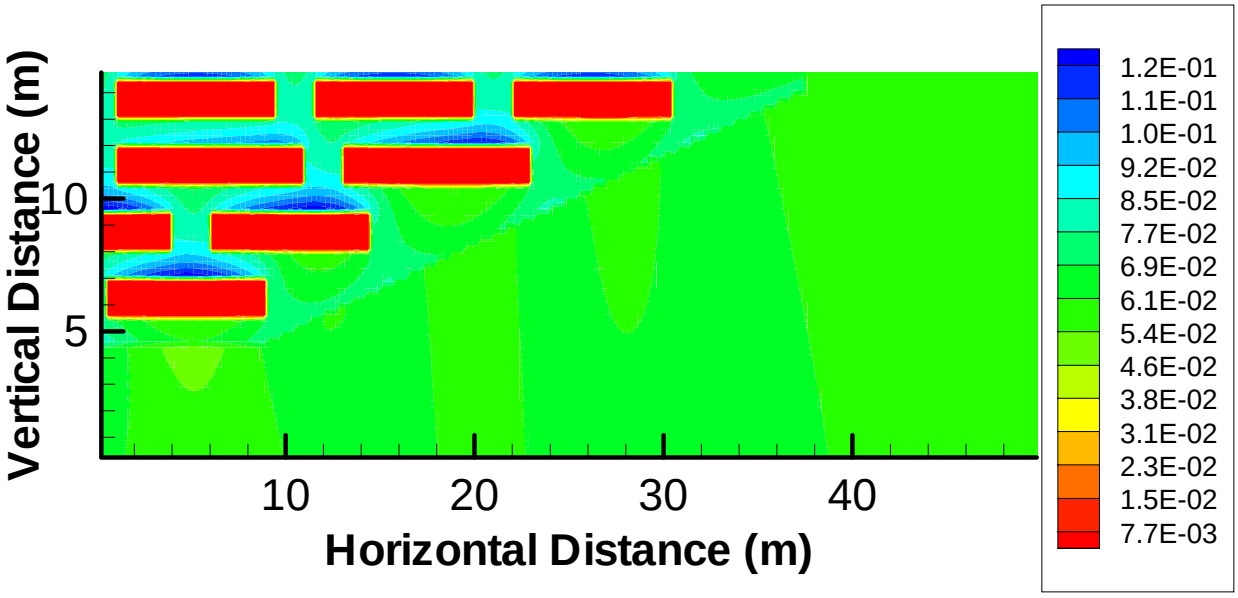

Figure 18. Volumetric Water Content for 2-D Trench Simulation

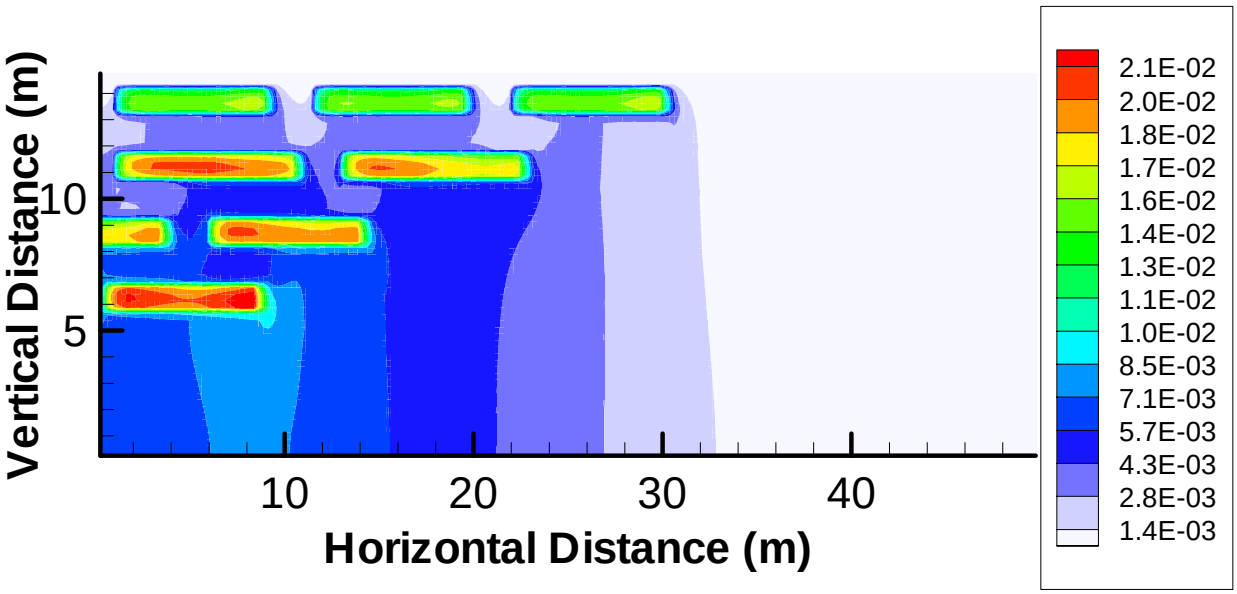

Figure 19. Total Aqueous Tc Concentration (μmol/kg) for 2-D Trench Simulation at 2,000 yr

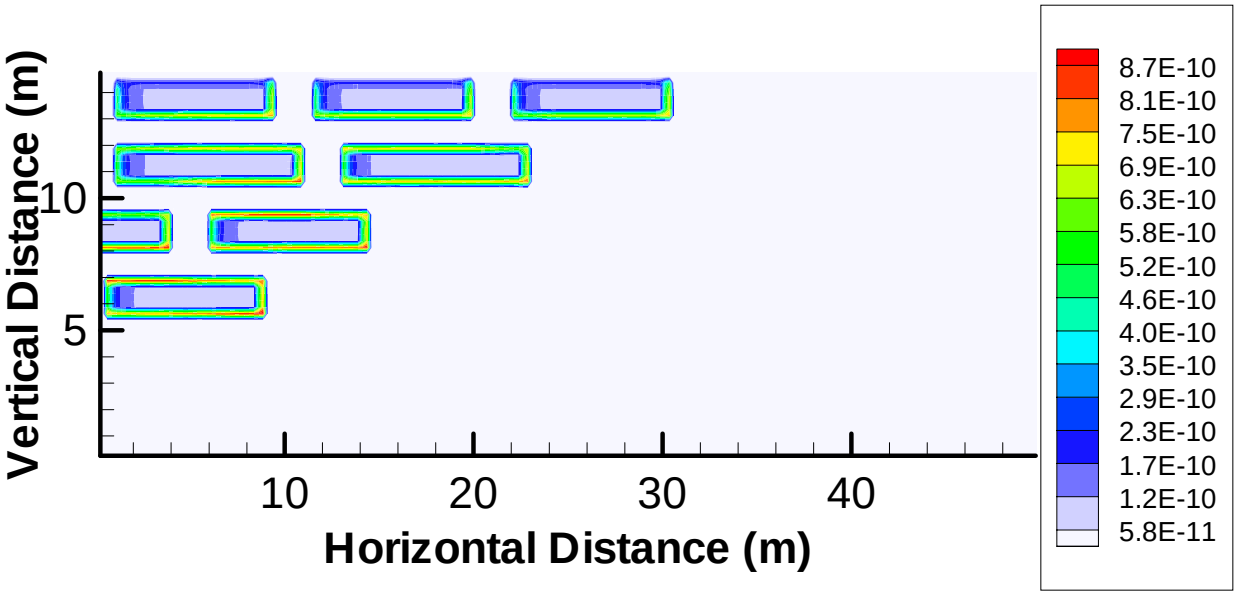

Figure 20. Glass Dissolution Rate (mol s^{-1}) for LAWABP1 in 2-D Trench Simulation at 2,000 yr

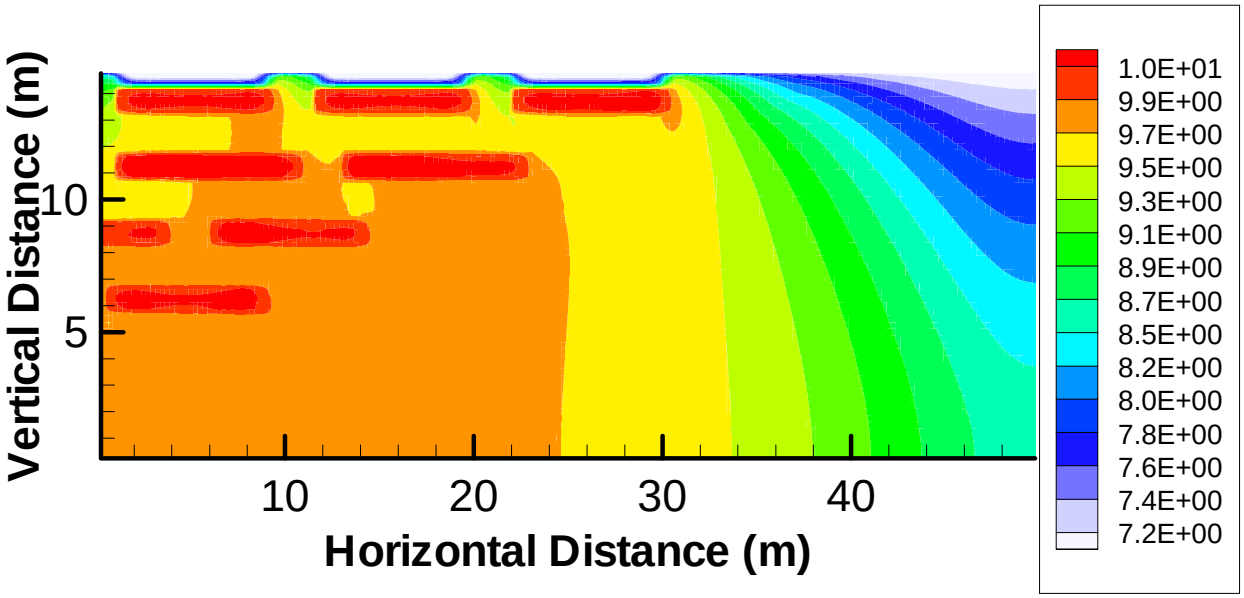

Figure 21. Solution pH for 2-D Trench Simulation

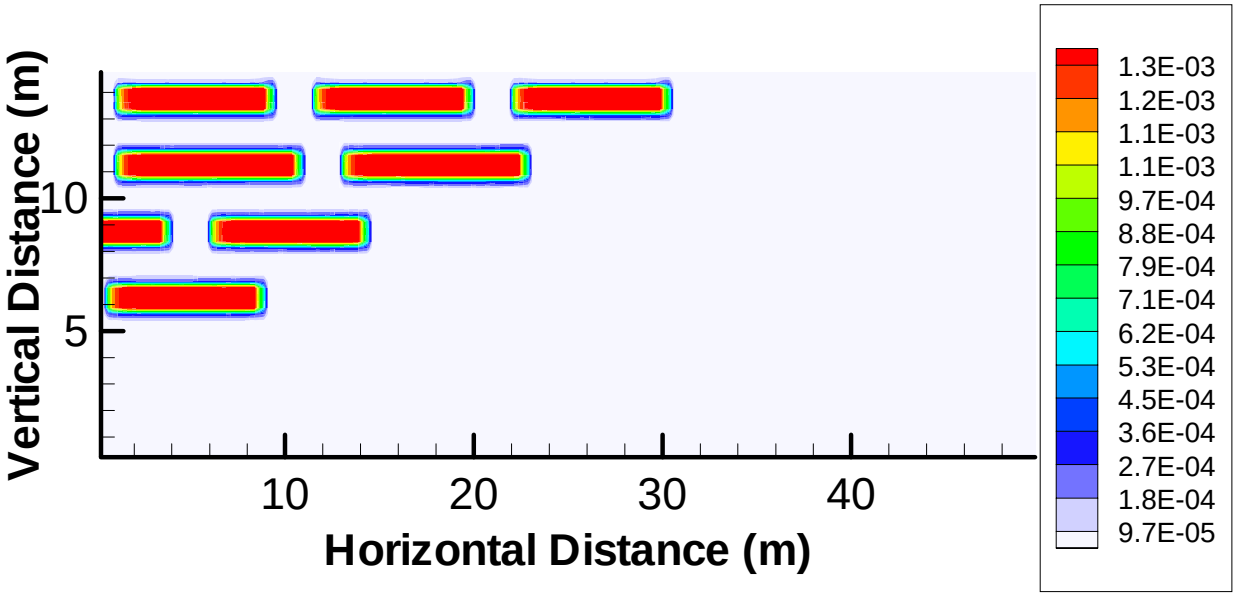

Figure 22. SiO_2(aq) Concentrations (mol/kg) for 2-D Trench Simulation

Vault Scenario

The normalized Tc flux to the vadose zone is 20% higher for the vault simulations than for the trench simulation at a recharge rate of 4.2 mm/yr (Figure 23). The glass packages are more closely packed in this simulation than in the trench simulation. This raises the pH inside the vault relative to the RH Trench simulation because there is less dilution available from the higher water contents in the intervening backfill layers (Figure 24). Substituting backfill for the degraded concrete has a negligible effect on the glass dissolution rate. Although the concrete layer causes an increase in pH as recharging waters enter (Figure 25), the glass layers cause a greater increase. As in the trench simulations, assuming lower recharge rates results in significantly smaller Tc flux to the vadose zone. The 0.1-mm/yr-recharge rate simulation was unable to progress past 1,800 yr because of high concentrations in the pore water percolating through the vault that caused convergence problems.

Extend Base Case to Water Table

This simulation is identical to the base case, except that the Hanford Sand layer was assumed to extend 88 m to the water table. Thus, the total depth of the model was 103 m for the extended grid, as opposed to 15 m for the base case simulation. Simulated pH (Figure 26) and TcO_4^- (Figure 27) concentrations for the upper 15 m of the extended simulation are very similar to those of the base case

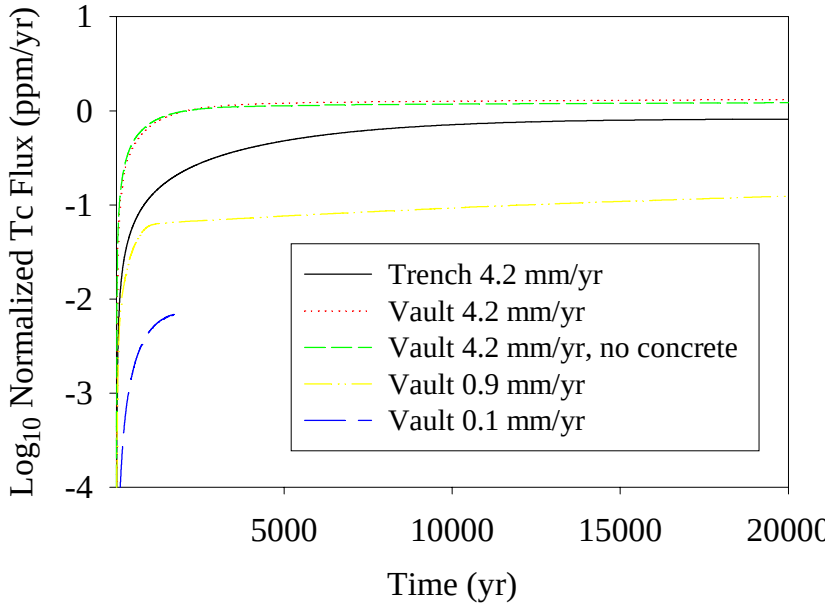

Figure 23. Tc Flux to the Vadose Zone, Relative to the Amount of Tc Originally in LAWABP1 Waste Glass, Comparison of Vault Simulations at Different Recharge Rates to Trench Base Case

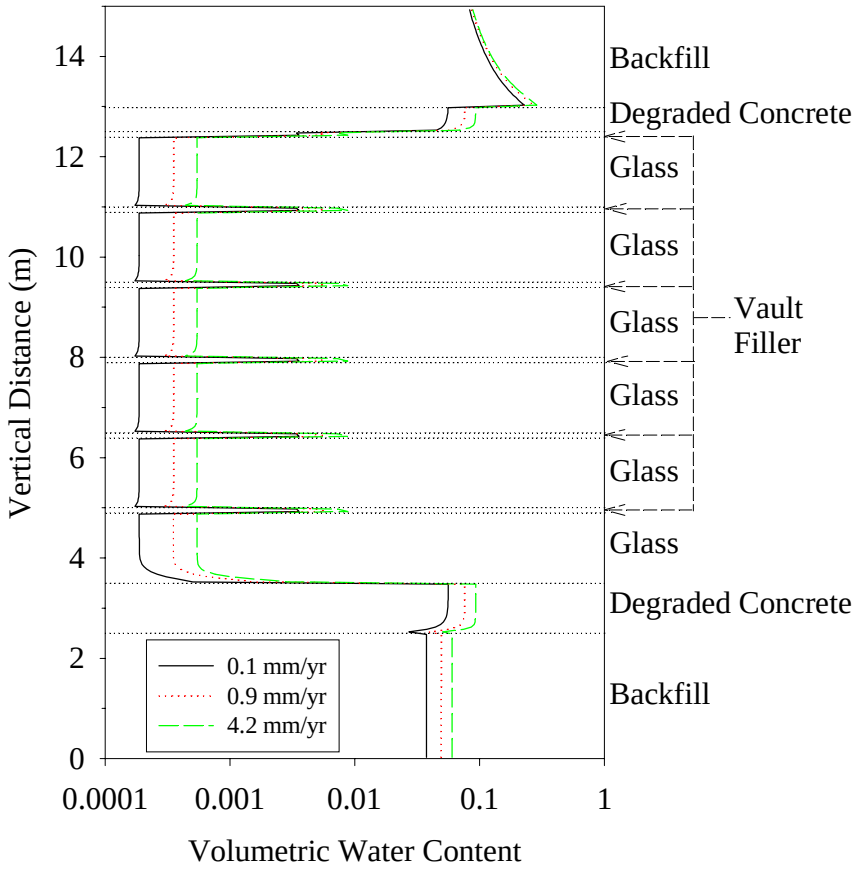

Figure 24. Water Contents for Selected Recharge Rates for Vault Simulations

until after 10,000 years, when the effect of the lower water table boundary begins to propagate up the profile. Even so, the Tc release rate is very similar for the base case and the extended simulation, the flux from the extended simulation being 7% lower at 1,000 years and 9% higher at 10,000 years than the base case. Longitudinal diffusion causes a decrease in the concentrations of aqueous species across the depth of the Hanford Sand. Solution pH decreases slightly from the top of the Hanford Sand to the water table (Figure 26). Aqueous TcO_4^- decreases from the top of the Hanford Sand to the water table by a factor of 3 at 2,000 yr. By 20,000 yr, the profile is closer to steady state, and the decrease in Tc from the top of the Hanford Sand to the water table is only 9%.

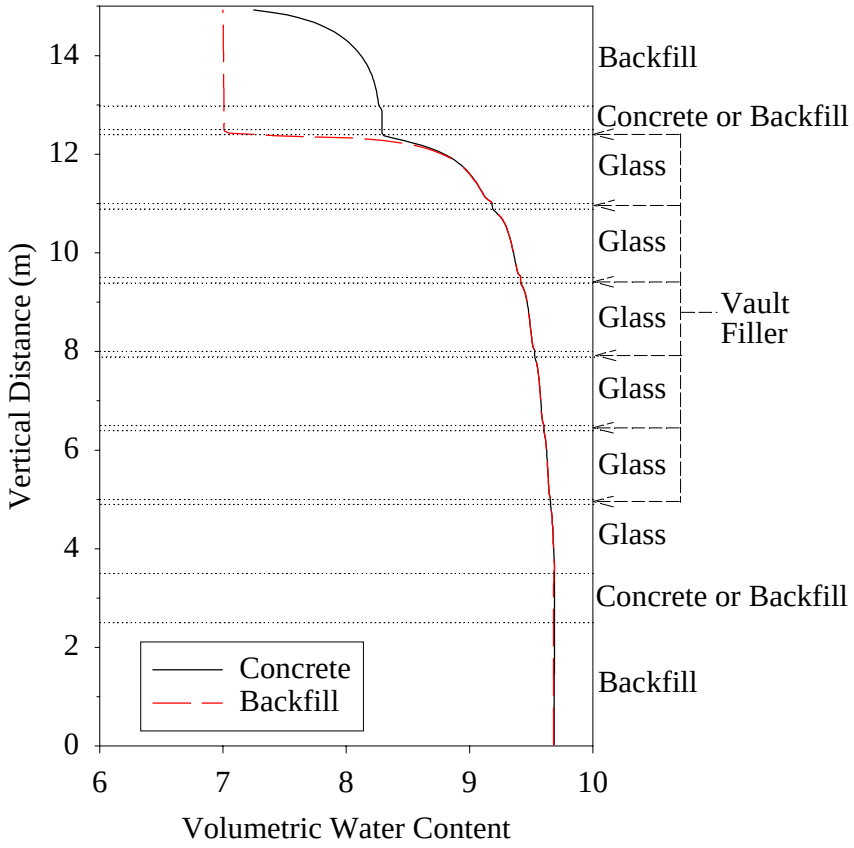

Figure 25. Effect of Concrete on pH for Vault Simulations

Bathtub Effect

This simulation considers the consequences of the trench liner being impermeable to flow, thus causing the trench to become saturated with water. The trench was initially considered to be saturated with water, with no flow across the bottom boundary. Simulated pH (Figure 28) and TcO_4^- concentrations are similar to those predicted by the base case. However, because the total amount of water in the profile is so much higher than for the base case, the total amount of Tc released is much higher.

Higher Waste Loading and Alternate Glass Formulation

The base analysis case uses a Na_2O waste loading of 20 weight percent. Increasing the Na_2O loading in LAW glasses has several impacts that can affect the long-term dissolution rate of the product. First, sodium is a glass "network breaker." Adding sodium to silicate glasses depolymerizes the glass, making its structure less interconnected and, so, generally less durable when contacted by water. Second, increased sodium content may make the glass more susceptible to alkali ion exchange reactions.

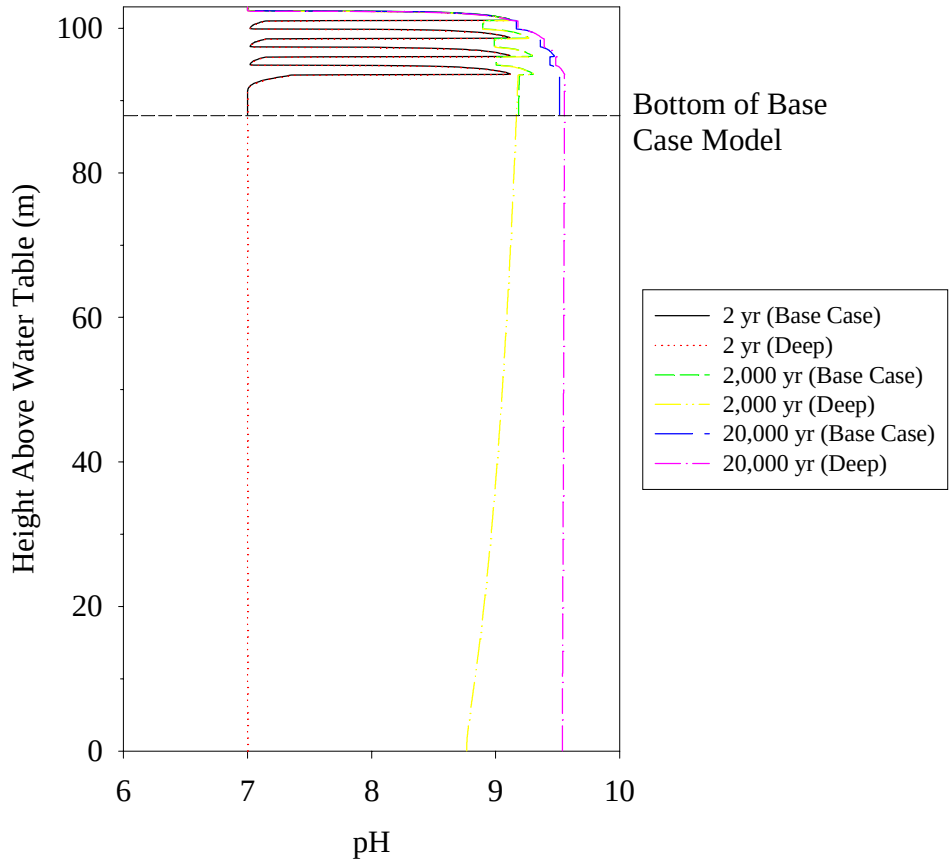

Figure 26. Solution pH Profile for RH Trench Simulation Extended to Water Table (See Figure 7 for location of boundaries between material zones and material names)

The net affect of ion exchange is to raise the pH of water percolating through the disposal system, thereby increasing the glass dissolution rate. Lastly, increasing the Na_2O content tends to expand the stability field and rate of zeolitic alteration phase formation as the glass reacts with water. Zeolite formation can cause dissolution rate excursions, sometimes all the way back to the forward rate of reaction. Thus, higher sodium loading will likely shrink the composition region from which acceptable LAW glasses can be formulated.

There is only a limited experimental base for LAW glasses at other than 20 weight percent Na_2O loading. From the limited data in Figure 30, a simple linear regression gives a slope of $10^{0.2x}$, where x is the mass percent Na_2O. Consequently, a 5 percent increase in Na_2O loading would increase the glass corrosion rate by approximately ten times. However, to conduct a more detailed analysis, laboratory experiments with HLP-31 glass (Vienna et al. 2000), which has a Na_2O loading of 23 weight percent, were performed to establish the necessary input parameters for STORM simulations. The results (see Figure 31) show a very unusual glass corrosion behavior in that the dissolution rate is apparently unaffected by an increasing concentration of silicon in the aqueous phase, up to near saturation with respect to amorphous silica. Also, the congruent release of Na and B indicates that little or no Na ion

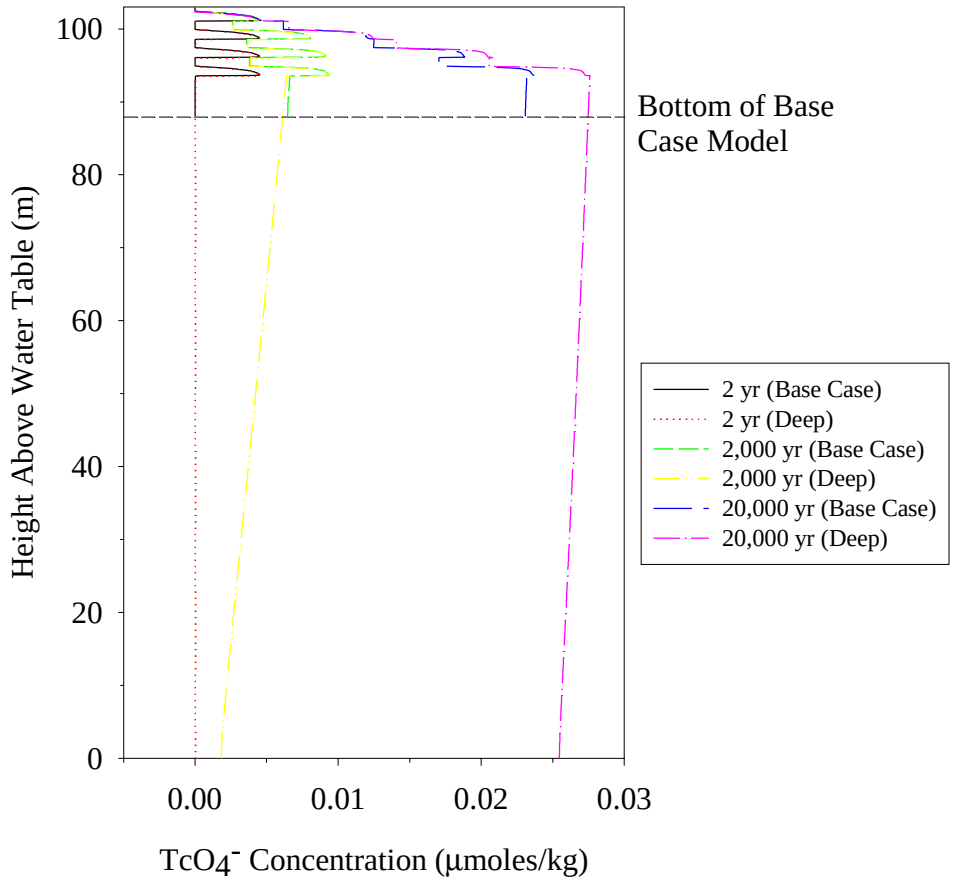

Figure 27. Concentration Profile of TcO_4^- for RH Trench Simulation Extended to Water Table (See Figure 4 for location of boundaries between material zones and material names)

exchange is occurring, despite the higher waste loading. Finally, the forward rate of reaction for this glass is about ten times larger than for LAWABP1 glass at the same temperature and pH. The reasons for this unusual behavior may be related to microscale phase separation as a result of the heat treatment used to simulate canister cooling (McGrail et al. 2001). In any event, to model the performance of this glass in the disposal system, the glass dissolution rate was not allowed to decrease as the Si concentration in the disposal system pore water increased. No experimental data was available on the pH-dependence of the dissolution rate so it was assumed that the reaction rate increased according to $10^{0.5*pH}$, identical to the power law determined for LAWABP1 glass.

The calculated normalized contaminant flux to the vadose zone for HLP-31 glass is 75 to 164 times larger (Table 13) than that for the base case simulation with LAWABP1 glass, as shown in Figure 32. The higher forward reaction rate of HLP-31 glass generates a higher calculated pH in the glass layers as compared with LAWABP1 glass. The combined effect of these factors, and the fact that the rate does not diminish with increasing Si concentration, increases the total release rate much more than the

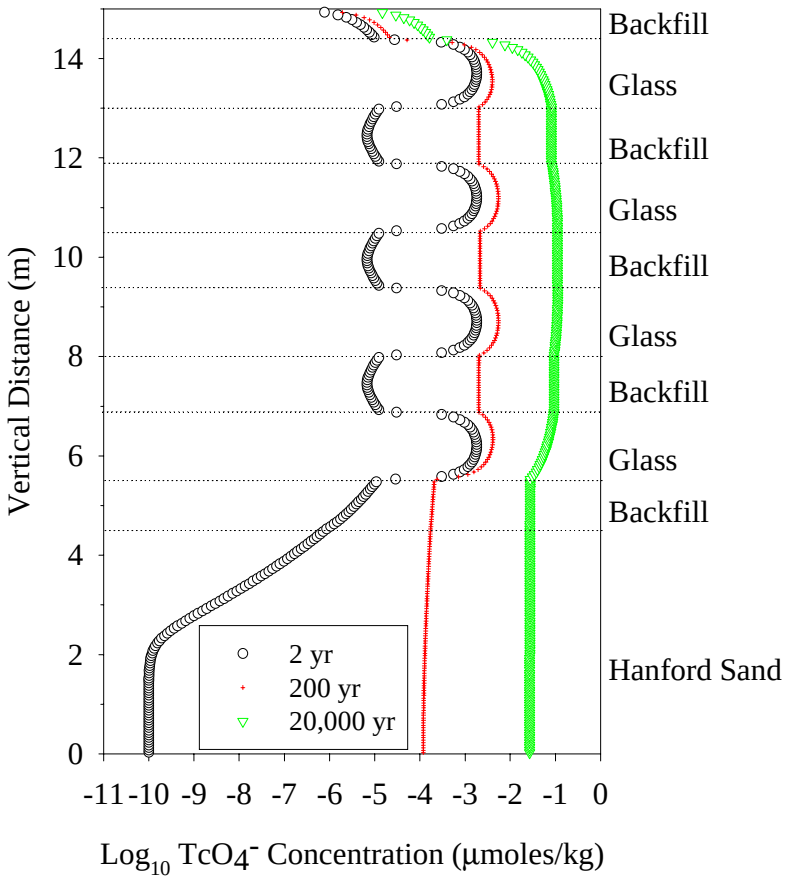

Figure 28. TcO_4^- for Fully-Saturated RH Trench Simulation with no Flow ("bathtub effect")

forward rate difference between the glasses alone would indicate. The decline in release rate after 5,000 years occurs because of the decreasing surface area of HLP-31 glass, which changed very little for the slower dissolving LAWABP1 glass over the same period.

The STORM simulations show the strong sensitivity of release rates to the durability of the glass. Available testing data indicate that Na_2O loadings of 20 to 25 weight percent might be achieved and still produce glasses that will have acceptable long-term performance. VHT testing shows several glasses at 23 weight percent Na_2O loading with a corrosion rate that is nearly as good as LAWABP1 glass (Vienna et al. 2000). Only very limited data at waste loadings above 25 weight percent Na_2O is available. Although it may be possible to formulate acceptable glasses at this waste loading, the acceptable glass composition region will be much smaller than is observed at waste loadings of 20 weight percent Na_2O and lower. Additional studies are needed if waste loadings approaching 25 weight percent Na_2O are desired. Major increases in waste loading on the order of 50 to 100 percent (30 to 40 weight percent Na_2O) are probably not possible with silicate-based glasses. A different glass-forming system, such as

the phosphate system, would need to be considered. However, changing to a different glass forming system would also require a different melter design, flow sheet, etc. Also, non-silicate waste glasses have received almost no attention since the early 1980's. Consequently, a significant research and development effort would be required to evaluate long-term performance issues with these glasses.

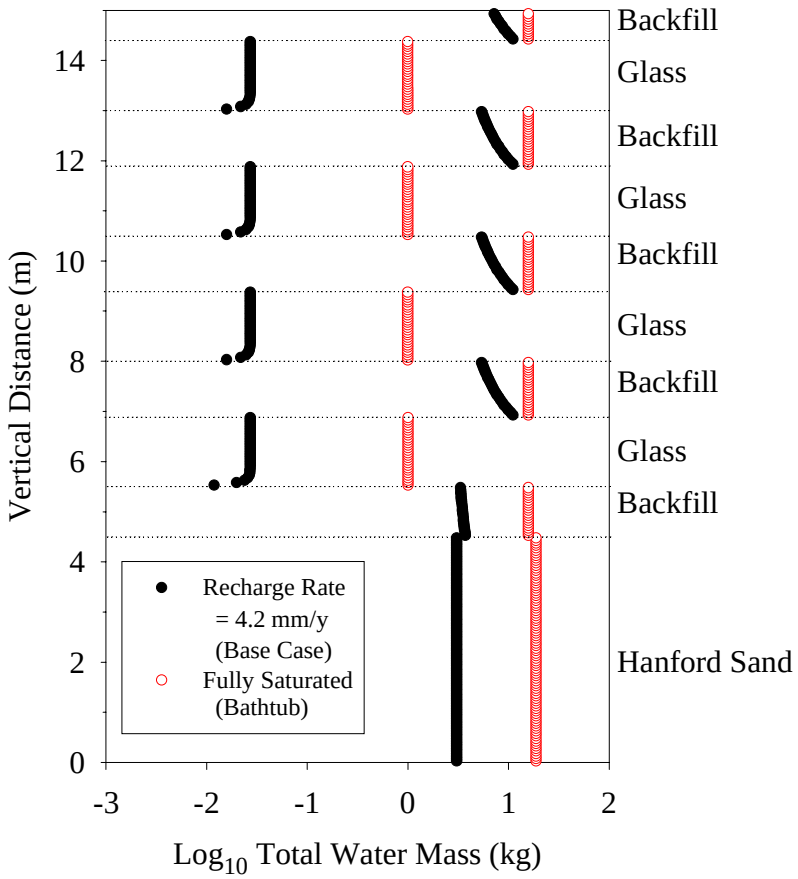

Figure 29. Total Water Mass per Node (each node has a volume of 0.05 m^3) for Fully-Saturated RH Trench Simulation with no Flow ("bathtub effect")

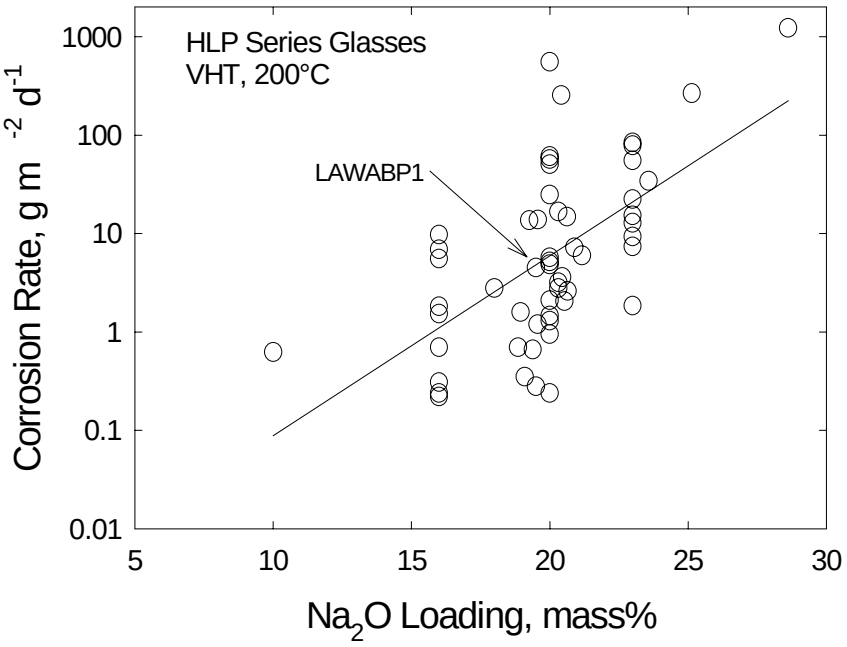

Figure 30. VHT Corrosion Rate as a Function of Waste Loading (Vienna et al. 2000)

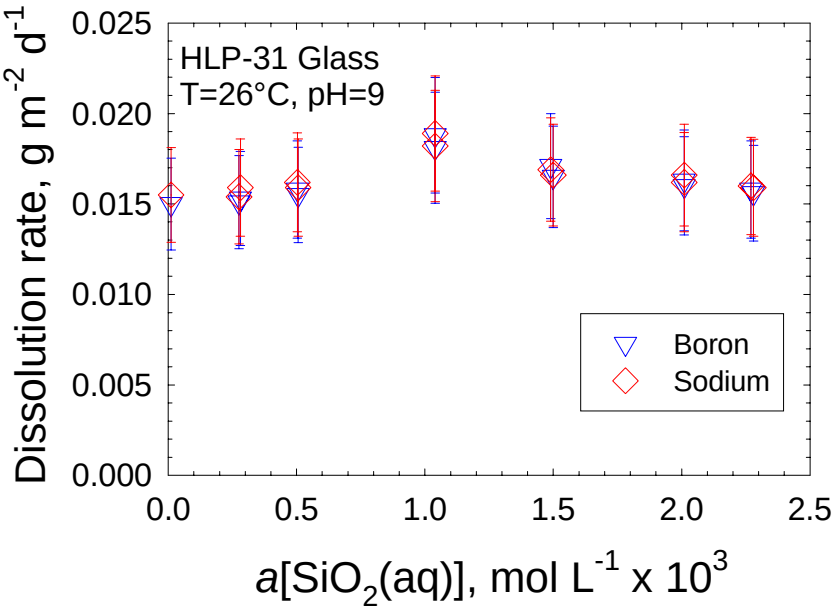

Figure 31. Dependence of HLP-31 Glass Dissolution Rate on Concentration of SiO_2(aq)

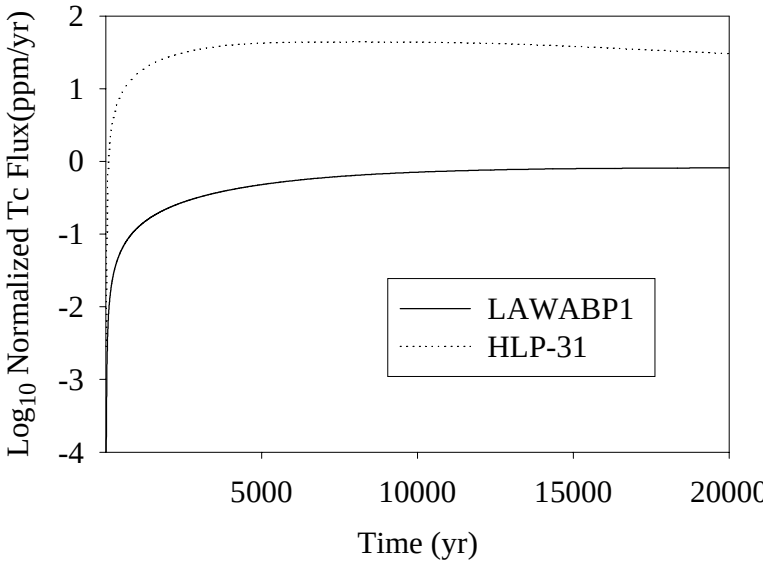

Figure 32. Tc Flux to the Vadose Zone, Relative to the Amount of Tc Originally in LAWABP1 Waste Glass, Comparison of Trench Base Case Simulation with LAWABP1 Glass Replaced by HLP-31 Waste Glass

Conclusion

The maximum normalized Tc release rate from the trench under a recharge rate of 4.2 mm/yr is 0.93 ppm/yr at 100,000 yr. The relevant performance objective of the disposal system for protecting groundwater resources is a beta-photon drinking water dose of no more than 4 mrem/yr (40 CFR 141 1975). Based on estimated transport to a well 100 m down gradient of the disposal facility (Mann et al. 2000), at a recharge rate of 4.2 mm/yr, the maximum allowable Tc release rate is 166 ppm/yr. The Tc release rate predicted by the base case simulation is 200 times less than the maximum allowable Tc release rate. Even the forward rate simulation, which has the highest predicted Tc release rates, is 25 times lower than the maximum allowable Tc release rate.

The sensitivity cases that have significantly higher normalized Tc release rates than the base case are the cases that consider: higher recharge rates, glass dissolution at forward rate of reaction, backfill replaced with sand, stainless steel mixed with glass, and the vault scenarios (Table 13). The sensitivity cases that have significantly lower normalized Tc release rates than the base case are the cases that consider: lower recharge rates, increased diffusion coefficient for all species, and the 2-D simulations. The sensitivity cases that are not significantly different than the base case are the cases that consider: no ion exchange, no secondary mineral formation, added conditioning layer at the top of the trench, stainless steel added at edges of glass layers, and U release. However, simulations including the stainless steel showed four orders of magnitude higher release rates of Cr(VI) due to the short release time relative to the glass and 100X higher inventory of Cr in the steel. In contrast, precipitation of theophrastite, $Ni(OH)_2$, limited Ni release rates to 1 to 3 orders of magnitude lower than those for Cr.

The results of these simulations display the complex interactions between the waste glass, native materials, and secondary minerals. The importance of having accurate rate constant data is shown by the difference between the base case and forward rate simulations. The need to accurately characterize the hydraulic properties of the materials in the disposal facility is shown by the significant effect of replacing the trench backfill material with sand. The importance of considering the proper spatial relationships between the different materials is highlighted by the 10X difference in Tc release between the two simulations where the stainless steel containers are treated as thin layers versus homogeneous mixing with the glass.

The exceedingly long time (months) required to conduct full 2-D simulations needs to be addressed if STORM is to be used for more extensive modeling studies. Improvements in execution speed can be obtained by implementing faster and more robust numerical algorithms to speed the rate of convergence and by substituting parallel algorithms for the principal time-consuming numerical routines in the code. This would allow execution of STORM on today's fastest massively parallel computers.

Table 13. Summary of Waste Form Sensitivity Calculations

Case	Description	Basic Model	Note	Radionuclide Flux Ratio @ 1,000 yr	Radionuclide Flux Ratio @ 10,000 yr	Reason Radionuclide Flux Ratio is Higher or Lower Than Base Case
WFA	4.2 mm/yr infiltration	Trench		1	1	This is the base case
WFB	Forward rate, 4.2 mm/yr infiltration	Trench		9.9	8.7	Forward rate
WFC	4.2 mm/yr infiltration	Vault		8.5	2.7	Vault, glass packed closer, higher pH
WFD	0.1 mm/yr infiltration	Trench		0.0004	0.0004	Lower recharge
WF1	Assume no Ion Exchange	Trench		0.8	0.8	Lower pH
WF2	Assume no Secondary Phase Formation	Trench		0.51	0.53	Higher Si concentration
WF4	0.9 mm/yr infiltration rate	Trench		0.016	0.016	Lower recharge
WF6	50 mm/yr infiltration rate	Trench		20.9	3.4	Higher recharge
WF7	0.5 mm/yr infiltration rate	Trench		0.005	0.004	Lower recharge
WF8	10 mm/yr infiltration rate	Trench		8.4	2.6	Higher recharge
WF9	Extend WFA to groundwater	Trench		0.93	1.09	Deeper lower boundary
WF10	Add conditioning layer at top	Trench		0.99	0.92	Higher Si concentration
WF11	Change filler material in trench to sand	Trench		9.1	1.6	Water content/diffusion higher in sand
WF14	Increase diffusion for all aqueous species by a factor of 10	Trench		0.06	0.01	Lower pH
WF16	Replace concrete everywhere with backfill material	Vault		9.1	2.5	Vault, glass packed closer, higher pH
WF19	0.9 mm/yr infiltration rate	Vault		0.75	0.20	Vault, lower recharge
WF21	0.1 mm/yr infiltration	Vault	Could not converge after 1,800 yr	0.055	-	Vault, lower recharge
WF25	Include steel in waste packages	Trench		1.03 (49,000)	1.02 (4,100)	Steel corrosion increases pH, note: values in parentheses are Cr flux ratios relative to base case
WF26	Replace Tc w/U	Trench		1.03	0.99	Soddyite precipitation
WF27	Full 2-D simulation	Trench	Could not converge after 2,000 yr	2.65	0.46	Lower water flux through glass
WF28/ WFx	Increase Waste Loading / Alternate Glass Formulation (HLP-31)	Trench	Could not converge after 5,500 yr	164	76	Higher release rate, no dependence on Si
WF30	Increase ion exchange rate by 5 times for WFB	Trench		12.17	9.51	Forward rate, higher pH

References

40 CFR 141. 1975. U.S. Environmental Protection Agency, "National Primary Drinking Water Regulations." *US Code of Federal Regulations*.

Bacon DH, MD White, and BP McGrail. 2000. *Subsurface Transport Over Reactive Multiphases (STORM): A General, Coupled, Nonisothermal Multiphase Flow, Reactive Transport, and Porous Medium Alteration Simulator, Version 2, User's Guide*. PNNL-13108, Pacific Northwest National Laboratory, Richland, Washington.

Cloke PL, DM Jolley, and DH Lester. 1997. *Waste Package Development Design Analysis*. BBA000000-01717-0200-0050 Rev. 00, CRWMS/M&O, Las Vegas, Nevada.

Daveler SA, and TJ Wolery. 1992. *EQPT, A Data File Preprocessor for the EQ3/6 Software Package: User's Guide and Related Documentation (Version 7.0)*. UCRL-MA-110662 PT II, Lawrence Livermore National Laboratory, Livermore, California.

Farnsworth RK, MKW Chan, and SC Slate. 1985. "The Effect of Radial Temperature Gradients on Glass Fracture in Simulated High-Level Waste Canisters." *Mat. Res. Soc. Symp. Proc.*, 44:831-838.

Fayer MJ, EM Murphy, JL Downs, FO Khan, CW Lindenmeier, and BN Bjornstad. 1999. *Recharge Data Package for the Immobilized Low-Activity Waste 2001 Performance Assessment*. PNNL-13033, Pacific Northwest National Laboratory, Richland, Washington.

Grenthe I, J Fuger, RJM Konings, RJ Lemire, AB Muller, C Nguyen-Trung, and H Wanner. 1992. *Chemical Thermodynamics, Volume 1: Chemical Thermodynamics of Uranium*. North-Holland, Amsterdam.

Jantzen C. 1984. "Methods of simulating low redox potential (Eh) for a basalt repository." *Mat. Res. Soc. Symp. Proc.*, 26:613-621.

Kaplan DI, and RJ Serne. 1999. *Geochemical Data Package for the Hanford Immobilized Low-Activity Tank Waste Performance Assessment (ILAW-PA)*. PNNL-13037, Pacific Northwest National Laboratory, Richland, Washington.

Khaleel R. 1999. *Far-Field Hydrology Data Package For Immobilized Low-Activity Tank Waste Performance Assessment*. HNF-4769, Rev. 1, Fluor Daniel Northwest, Inc., Richland, Washington.

Krupka KM, and RJ Serne. 1998. *Effects on Radionuclide Concentrations by Cement/Ground-Water Interactions in Support of Performance Assessment of Low-Level Radioactive Wate Disposal Facilities*. PNNL-11408, NUREG/CR-6377, Pacific Northwest National Laboratory, Richland, Washington.

Mann FM, SH Finfrock, EJ Freeman, RJ Puigh, II, DH Bacon, MP Bergeron, BP McGrail, and SK Wurstner. 2000. *White Paper Updating Conclusions of 1998 ILAW Performance Assessment*. DOE/ORP-2000-07 Rev. 0, Department of Energy, Office of River Protection, Richland, Washington.

Mann FM, RJ Puigh, II, CR Eiholzer, Y Chen, NW Kline, AH Lu, BP McGrail, PD Rittmann, GF Williamson, NR Brown, and PE LaMont. 1998. *Hanford Immobilized Low Activity Tank Waste Performance Assessment*. DOE/RL-97-69 Rev. B, Project Hanford Management Contractor, Richland, Washington.

McGrail B. 1986. "Waste package component interactions with Savannah River defense waste glass in a low-magnesium salt brine." *Nuc. Tech.*, 75(2):168-186.

McGrail BP, and DH Bacon. 1998. *Selection of a Computer Code for Hanford Low-Level Waste Engineered-System Performance Assessment*. PNNL-10830 Rev. 1, Pacific Northwest National Laboratory, Richland, Washington.

McGrail BP, DH Bacon, JP Icenhower, WL Ebert, PF Martin, HT Schaef, and EA Rodriguez. 2000. *Waste Form Release Data Package for the 2001 Immobilized Low-Activity Waste Performance Assessment*. PNNL-13043, Rev. 1, Richland, Washington.

McGrail BP, DH Bacon, JP Icenhower, WL Ebert, PF Martin, HT Schaef, and EA Rodriguez. 2001. *Waste Form Release Data Package for the 2001 Immobilized Low-Activity Waste Performance Assessment*. PNNL-13043, Rev. 2, Richland, Washington.

Meyer PD, and RJ Serne. 1999. *Near Field Hydrology Data Package for the Immobilized Low-Activity Waste 2001 Performance Assessment*. PNNL-13035, Richland, Washington.

Peters RD, and SC Slate. 1981. "Fracturing of Simulated High-Level Waste Canisters." *Nuc. Eng. Design*, 67:425-445.

Puigh R. 1999. *Disposal Facility Data for the Hanford Immobilized Low-Activity Tank Waste*. HNF 4950 Rev. 0, Washington, Richland.

Shock EL, and HC Helgeson. 1988. "Calculation of the thermodynamic and transport properties of aqueous species at high pressures and temperatures: Correlation algorithms for ionic species and equation of state predictions to 5kb and 1000°C." *Geochim. Cosmochim. Acta*, 52:2009-2036.

Shock EL, HC Helgeson, and DA Sverjensky. 1989. "Calculation of the thermo-dynamic and transport properties of aqueous species at high pressures and temperatures: Standard partial molal properties of inorganic neutral species." *Geochim. Cosmochim. Acta*, 53:2157-2183.

Sverjensky D, and N Sahai. 1996. "Theoretical prediction of single-site surface-protonation equilibrium constants for oxides and silicates in water." *Geochim. Cosmochim. Acta*, 60:3773-3797.

Vienna JD, A Jiricka, BP McGrail, BM Jorgensen, DE Smith, BR Allen, JC Marra, DK Peeler, KG Brown, IA Reamer, and WL Ebert. 2000. *Hanford Immobilized LAW Product Acceptance Testing: Initial Data Package*. PNNL-13101, Pacific Northwest National Laboratory, Richland, Washington.

Wolery TJ, and SA Daveler. 1992. *EQ6, A Computer Program for Reaction Path Modeling of Aqueous Geochemical Systems: Theoretical Manual, User's Guide, and Related Documentation (Version 7.0)*. UCRL-MA-110662 PT IV, Lawrence Livermore National Laboratory, Livermore, California.

Wootan DW. 1999. *Immobilized Low-activity Tank Waste Inventory Data Package*. HNF-4921, Rev. 0, Fluor Daniel Northwest, Inc., Richland, Washington.

Distribution

No. of Copies

OFFSITE

Argonne National Laboratory
Building 205
9700 South Cass Avenue
Argonne, IL 60439-4837
ATTN: W. L. Ebert

Lawrence Berkeley National Laboratory
Earth Sciences Division
University of California
Berkeley, CA 94720
ATTN: K. Pruess

2 Lawrence Livermore National Laboratory
University of California
7000 East Avenue
Livermore, CA 94550-9234
ATTN: T. J. Wolery, Mailcode L-219
W. E. Glassley, Mailcode L-202

Penn State University
College of Engineering
0212 Sackett Building
University Park, PA 16802
ATTN: G.-T. Yeh

4 Yucca Mountain Site Characterization Program
TRW Environmental Safety System
1180 Town Center Drive
Mail Stop 423
Las Vegas, NV 89134
ATTN: R. Andrews
E. Bartlett Mann
J. Lee
Y. Chen

No. of Copies

ONSITE

4 **DOE Richland Operations Office**

C. A. Babel	H6-60
N. R. Brown	H6-60
P. E. Lamont	H6-60
Public Reading Room	H2-53

3 **Bechtel Hanford, Inc.**

G. A. Jewell (2)	H0-21
B. H. Ford	H0-19

Lockheed Martin Hanford Corporation

J. A. Voogd	H6-64

11 **Fluor Federal Services**

D. A. Burbank	S4-45
K. C. Burgard	S4-45
T. A. Carlson	B4-09
S. H. Finfrock	B4-43
R. Khaleel	B4-43
F. M. Mann (2)	H0-22
M. G. Piepho	R3-26
R. J. Puigh	B4-43
R. W. Root	R2-53
P. D. Rittmann	B4-43

No. of Copies		
27	**Pacific Northwest National Laboratory**	
	M. P. Bergeron	K9-36
	R. W. Bryce	K6-75
	D. H. Bacon (5)	K9-33
	M. J. Fayer	K9-33
	E. J. Freeman	K9-33
	C. T. Kincaid	K9-33
	P. D. Meyer	BPO
	B. P. McGrail (5)	K6-81
	W. E. Nichols	K9-33
	M. D. White	K9-36
	S. K. Wurstner	K9-36
	S. B. Yabusaki	K9-36
	Information Release Office (7)	K1-06